











# TECH BRIEFS

NATIONAL AERONAUTICS AND SPACE ADMINISTRATION

-  **Technology Focus**
-  **Electronics/Computers**
-  **Software**
-  **Materials**
-  **Mechanics/Machinery**
-  **Manufacturing**
-  **Bio-Medical**
-  **Physical Sciences**
-  **Information Sciences**
-  **Books and Reports**



## INTRODUCTION

Tech Briefs are short announcements of innovations originating from research and development activities of the National Aeronautics and Space Administration. They emphasize information considered likely to be transferable across industrial, regional, or disciplinary lines and are issued to encourage commercial application.

### Availability of NASA Tech Briefs and TSPs

Requests for individual Tech Briefs or for Technical Support Packages (TSPs) announced herein should be addressed to

#### National Technology Transfer Center

Telephone No. (800) 678-6882 or via World Wide Web at [www.nttc.edu](http://www.nttc.edu)

Please reference the control numbers appearing at the end of each Tech Brief. Information on NASA's Innovative Partnerships Program (IPP), its documents, and services is also available at the same facility or on the World Wide Web at <http://ipp.nasa.gov>.

Innovative Partnerships Offices are located at NASA field centers to provide technology-transfer access to industrial users. Inquiries can be made by contacting NASA field centers listed below.

## NASA Field Centers and Program Offices

#### Ames Research Center

Lisa L. Lockyer  
(650) 604-1754  
[lisa.l.lockyer@nasa.gov](mailto:lisa.l.lockyer@nasa.gov)

#### Dryden Flight Research Center

Gregory Poteat  
(661) 276-3872  
[greg.poteat@dfrc.nasa.gov](mailto:greg.poteat@dfrc.nasa.gov)

#### Glenn Research Center

Kathy Needham  
(216) 433-2802  
[kathleen.k.needham@nasa.gov](mailto:kathleen.k.needham@nasa.gov)

#### Goddard Space Flight Center

Nona Cheeks  
(301) 286-5810  
[nona.k.cheeks@nasa.gov](mailto:nona.k.cheeks@nasa.gov)

#### Jet Propulsion Laboratory

Ken Wolfenbarger  
(818) 354-3821  
[james.k.wolfenbarger@jpl.nasa.gov](mailto:james.k.wolfenbarger@jpl.nasa.gov)

#### Johnson Space Center

Michele Brekke  
(281) 483-4614  
[michele.a.brekke@nasa.gov](mailto:michele.a.brekke@nasa.gov)

#### Kennedy Space Center

David R. Makufka  
(321) 867-6227  
[david.r.makufka@nasa.gov](mailto:david.r.makufka@nasa.gov)

#### Langley Research Center

Martin Waszak  
(757) 864-4015  
[martin.r.waszak@nasa.gov](mailto:martin.r.waszak@nasa.gov)

#### Marshall Space Flight Center

Jim Dowdy  
(256) 544-7604  
[jim.dowdy@msfc.nasa.gov](mailto:jim.dowdy@msfc.nasa.gov)

#### Stennis Space Center

John Bailey  
(228) 688-1660  
[john.w.bailey@nasa.gov](mailto:john.w.bailey@nasa.gov)

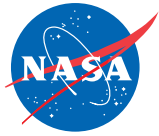
#### Carl Ray, Program Executive

Small Business Innovation  
Research (SBIR) & Small  
Business Technology  
Transfer (STTR) Programs  
(202) 358-4652  
[carl.g.ray@nasa.gov](mailto:carl.g.ray@nasa.gov)

#### Doug Comstock, Director

Innovative Partnerships  
Program Office  
(202) 358-2560  
[doug.comstock@nasa.gov](mailto:doug.comstock@nasa.gov)





# TECH BRIEFS

NATIONAL AERONAUTICS AND SPACE ADMINISTRATION



## 5 Technology Focus: Composites and Coatings

- 5 Wirelessly Interrogated Position or Displacement Sensors
- 6 Ka-Band Radar Terminal Descent Sensor
- 6 Metal/Metal Oxide Differential Electrode pH Sensors
- 7 Improved Sensing Coils for SQUIDs
- 8 Inductive Linear-Position Sensor/Limit-Sensor Units



## 9 Electronics/Computers

- 9 Hilbert-Curve Fractal Antenna With Radiation-Pattern Diversity
- 10 Single-Camera Panoramic-Imaging Systems
- 11 Interface Electronic Circuitry for an Electronic Tongue
- 12 Inexpensive Clock for Displaying Planetary or Sidereal Time
- 13 Efficient Switching Arrangement for  $(N + 1)/N$  Redundancy
- 14 Lightweight Reflectarray Antenna for 7.115 and 32 GHz
- 15 Opto-Electronic Oscillator Using Suppressed Phase Modulation
- 16 Alternative Controller for a Fiber-Optic Switch



## 19 Materials

- 19 Strong, Lightweight, Porous Materials
- 19 Nanowicks
- 20 Lightweight Thermal Protection System for Atmospheric Entry



## 23 Manufacturing & Prototyping

- 23 Rapid and Quiet Drill
- 24 Hydrogen Peroxide Concentrator

## 27 Semiconductors & ICs

- 27 MMIC Amplifiers for 90 to 130 GHz



## 29 Mechanics/Machinery

- 29 Robot Would Climb Steep Terrain
- 29 Measuring Dynamic Transfer Functions of Cavitating Pumps



## 31 Bio Medical

- 31 Advanced Resistive Exercise Device
- 31 Rapid Engineering of Three-Dimensional, Multicellular Tissues With Polymeric Scaffolds

## 33 Physical Science



- 33 Resonant Tunneling Spin Pump
- 33 Enhancing Spin Filters by Use of Bulk Inversion Asymmetry
- 34 Optical Magnetometer Incorporating Photonic Crystals
- 35 WGM-Resonator/Tapered-Waveguide White-Light Sensor Optics
- 36 Raman-Suppressing Coupling for Optical Parametric Oscillator
- 37 CO<sub>2</sub>-Reduction Primary Cell for Use on Venus
- 37 Cold Atom Source Containing Multiple Magneto-Optical Traps



## 39 Information Sciences

- 39 POD Model Reconstruction for Gray-Box Fault Detection
- 39 System for Estimating Horizontal Velocity During Descent



## 41 Software

- 41 Software Framework for Peer Data-Management Services
- 41 Autogen Version 2.0
- 41 Tracking-Data-Conversion Tool
- 41 NASA Enterprise Visual Analysis
- 42 Advanced Reference Counting Pointers for Better Performance
- 42 C Namelist Facility
- 42 Efficient Mosaicking of Spitzer Space Telescope Images

This document was prepared under the sponsorship of the National Aeronautics and Space Administration. Neither the United States Government nor any person acting on behalf of the United States Government assumes any liability resulting from the use of the information contained in this document, or warrants that such use will be free from privately owned rights.





## Wirelessly Interrogated Position or Displacement Sensors

These sensors could be used in harsh environments.

Langley Research Center, Hampton, Virginia

Two simple position or displacement sensors based on inductance-capacitance resonant circuits have been conceived. These sensors are both powered and interrogated without use of wires and without making contact with other objects. Instead, excitation and interrogation are accomplished by means of a magnetic-field-response recorder — an apparatus previously reported in “Magnetic-Field-Response Measurement-Acquisition System” (LAR-16908), *NASA Tech Briefs*, Vol. 30, No. 6 (June 2006), page 28. To recapitulate: The magnetic-field-response recorder generates an alternating magnetic field that excites oscillations in the resonant circuit, measures the magnetic response of the circuit, and determines the resonance frequency from the response.

Both of the present position or displacement sensors consist essentially of variable rectangular parallel-plate capacitors electrically connected in series with fixed inductors. In the first sensor,

(see Figure 1), the perpendicular distance,  $x$ , between the plates is variable and is the distance that one seeks to measure; alternatively, a change in this distance is the displacement that one seeks to measure. From the basic equations for the resonance angular frequency  $\omega$  of an inductance-capacitance circuit and a first order approximation (fringing field neglected) of a parallel-plate capacitor, it can readily be shown that the distance is related to the resonance frequency by

$$x = \frac{L\epsilon_0 kw}{\omega^2}$$

where  $L$  is the inductance,  $\epsilon_0$  is the vacuum permittivity, and  $l$  and  $w$  are the dimensions of the capacitor plates as indicated in Figure 1.

In the second sensor (see Figure 2), capacitor plates are constrained to remain at a perpendicular distance  $d$ , and one of the plates is free to slide parallel to the other one. The space between the

plates is filled with a dielectric material of relative permittivity  $\kappa$ . In this case, the distance,  $x$ , that one seeks to measure is the length by which the plates overlap. Using the same approximations as those for the first sensor, it can be shown that the overlap length is related to the resonance frequency by

$$x = \frac{d}{\omega^2 L \kappa \epsilon_0 k w}$$

Simple inductance-capacitance circuits of the type used in these sensors are inherently robust; their basic mode of operation does not depend on maintenance of specific environmental conditions. Hence, these sensors can be used under such harsh conditions as cryogenic temperatures, high pressures, and radioactivity.

*This work was done by Stanley E. Woodard of Langley Research Center and Bryant D. Taylor of Swales Aerospace. For further information, contact the Langley Innovative Partnerships Office at (757) 864-8881. LAR-16617-1*

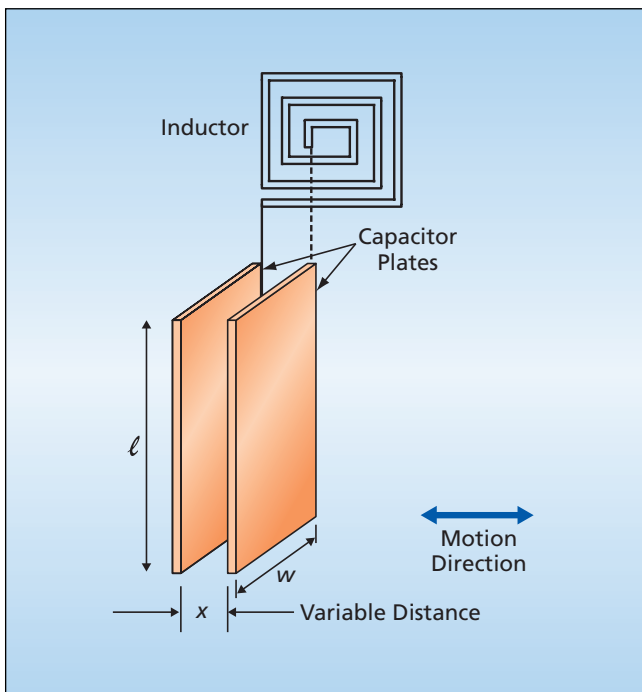


Figure 1. The **Distance Between the Plates** of a capacitor in a capacitor-inductor resonant circuit is varied. The distance can be calculated as a known function of the measured resonance frequency.

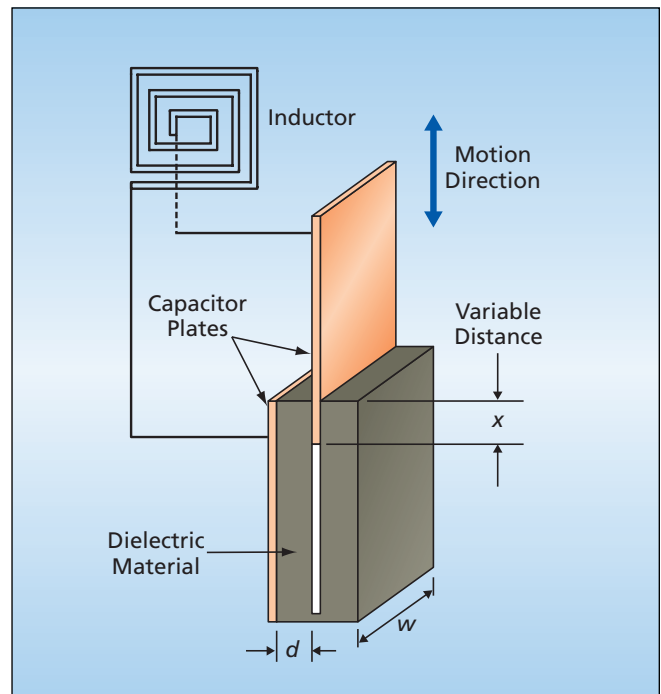


Figure 2. The **Length of Overlap of the Plates** of a capacitor in a capacitor-inductor resonant circuit is varied. As in the case of Figure 1, this length can be calculated as a known function of the measured resonance frequency.

## Ka-Band Radar Terminal Descent Sensor

**Radar altimeter/velocimeter improves velocity sensing by an order of magnitude and eliminates angle-of-descent errors.**

*NASA's Jet Propulsion Laboratory, Pasadena, California*

The terminal descent sensor (TDS) is a radar altimeter/velocimeter that improves the accuracy of velocity sensing by more than an order of magnitude when compared to existing sensors. The TDS is designed for the safe planetary landing of payloads, and may be used in helicopters and fixed-wing aircraft requiring high-accuracy velocity sensing.

The TDS uses 35.75-GHz frequency to optimize accuracy without requiring new technology, and incorporates a millimeter-wave center frequency to eliminate angle-of-arrival errors that can result in large velocity errors over non-homogeneous terrain. A memory-less approach to altimetry reacquires the target on each beam for each unique measurement, overcoming problems of ambiguous measurements or high dynamics that have plagued previous altimeter designs. The independent beam-to-beam and repeat-beam performance avoids "loss of lock" problems, as well as any issue where the heat shield, or an anomaly of some sort, might put the radar in a false state.

The "sky-crane" concept developed for the 2009 Mars Science Laboratory (MSL) mission allows the delivery of much larger payloads than the previ-



The TDS RF Design consists of a receiver rack drawer, a frequency synthesizer rack drawer, and an upconverter/downconverter.

ously developed airbag landing methods, and it overcomes the problems of egress that pallet landers traditionally have faced. The system requires high-accuracy velocity on a minimum of three independent beams, high-accuracy slant range measurements on all velocimeter beams, and performance over an aggressive range of vehicle dynamics, includ-

ing high altitude excursions, high attitude rates, and high attitude vehicle velocities. Also necessary are knowledge and control of the touchdown vehicle velocity: the MSL rover requires less than 1.5-m/s vertical and 0.75-m/s horizontal velocities at touchdown. This altimeter/velocimeter innovation can meet these needs, enabling the sky-crane concept.

At the time of this reporting, the TDS was in breadboard form, and was a single-channel, Ka-band model created with a commercial-off-the shelf (COTS) antenna, connectorized RF components, miniature Ka-band RF hybrids in small, connectorized packages for the T/R module, and a LabVIEW/laptop interface. The RF design is shown in the figure. The equipment has been verified with bench testing that included short-pulse generation, Doppler/velocity product generation, FPGA (field-programmable-gate-array) timing, RF power levels, and RF passband response.

*This work was done by Brian Pollard, Andrew Berkun, Michael Tope, Constantine Andricos, Joseph Okonek, and Yunling Lou of Caltech for NASA's Jet Propulsion Laboratory. Further information is contained in a TSP (see page 1). NPO-44462*

## Metal/Metal Oxide Differential Electrode pH Sensors

**These sensors are rugged, and reference solutions are not needed.**

*NASA's Jet Propulsion Laboratory, Pasadena, California*

Solid-state electrochemical sensors for measuring the degrees of acidity or alkalinity (in terms of pH values) of liquid solutions are being developed. These sensors are intended to supplant older electrochemical pH sensors that include glass electrode structures and reference solutions. The older sensors are fragile and subject to drift. The present developmental solid-state sensors are more rugged and are expected to be usable in harsh environments.

Like the older electrochemical pH sensors, the present sensors are based on a differential-electrode measurement principle. Each sensor includes two electrodes, made of different materials, in equilibrium

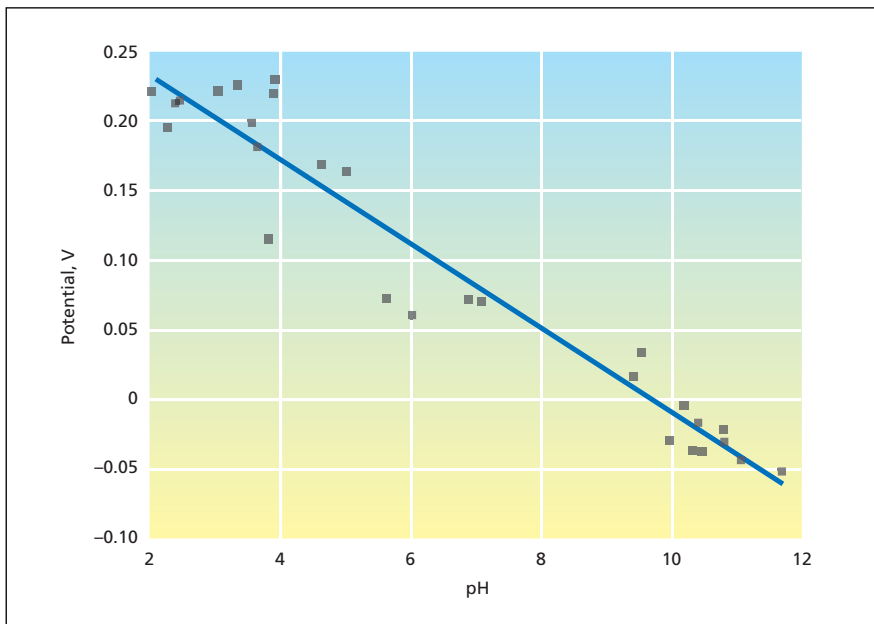
with the solution of interest. The electrode materials are chosen so that the electric potential of one electrode is sensitive (or more sensitive) to the pH of the solution of interest while the electric potential of the other electrode is insensitive (or less sensitive) to the pH of the solution. One measures the difference between the potentials on the two electrodes and deduces the pH from the known relationship between that difference and the pH.

One of the electrodes of a pH sensor of the present type is an iridium wire that has been partially oxidized to have a surface layer of iridium oxide about 15  $\mu\text{m}$  thick. The other electrode is a rhodium foil that has been similarly treated to im-

part a surface layer of rhodium oxide about 5  $\mu\text{m}$  thick.

In calibration tests, the dependence of the electric potential of the iridium/iridium oxide electrode upon pH was found to closely approximate that predicted by the Nernst equation, at a slope between  $-57$  and  $-59$  mV/pH. The dependence of the electric potential of the rhodium/rhodium oxide electrode upon pH was found to be sub-Nernstian, at a slope of about  $-26$  mV/pH. Hence, in constructing a pH sensor, iridium/iridium oxide was used for the sensing (more-sensitive) electrode and rhodium/rhodium oxide for the reference (less-sensitive) electrode. When the difference between





Differences Between the Potentials of an iridium/iridium oxide electrode and a rhodium/rhodium oxide electrode were measured when the electrodes were in equilibrium with solutions having several different pH values.

the potentials of the two electrodes was measured as a function of pH, the slope was found to be about  $-30 \text{ mV/pH}$  (see figure). This slope is well within the range of typical instrumentation used in converting DC signals to digital data for recording.

*This work was done by William West, Martin Buehler, and Didier Keymeulen of Caltech for NASA's Jet Propulsion Laboratory.*

*In accordance with Public Law 96-517, the contractor has elected to retain title to this invention. Inquiries concerning rights for its commercial use should be addressed to:*

*Innovative Technology Assets Management*

*JPL*

*Mail Stop 202-233*

*4800 Oak Grove Drive*

*Pasadena, CA 91109-8099*

*(818) 354-2240*

*E-mail: iaoffice@jpl.nasa.gov*

*Refer to NPO-43338, volume and number of this NASA Tech Briefs issue, and the page number.*

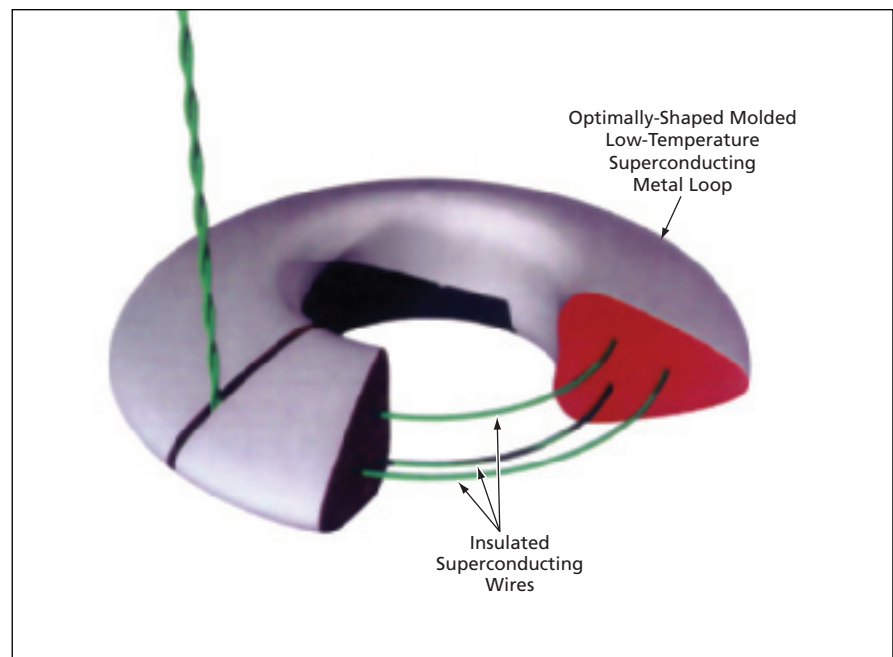
## Improved Sensing Coils for SQUIDS

Coils would be molded on outer surfaces of forms encapsulating superconducting wires.

NASA's Jet Propulsion Laboratory, Pasadena, California

An improvement in the design and fabrication of sensing coils of superconducting quantum interference device (SQUID) magnetometers has been proposed to increase sensitivity. It has been estimated that, in some cases, it would be possible to increase sensitivity by about half or to reduce measurement time correspondingly.

The pertinent aspects of the problems of design and fabrication can be summarized as follows: In general, to increase the sensitivity of a SQUID magnetometer, it is necessary to maximize the magnetic flux enclosed by the sensing coil while minimizing the self-inductance of this coil. It is often beneficial to fabricate the coil from a thicker wire to reduce its self-inductance. Moreover, to optimize the design of the coil with respect to sensitivity, it may be necessary to shape the wire to other than a commonly available circular or square cross-section. On the other hand, it is not practical to use thicker superconducting wire for the entire superconducting circuit, especially if the design of a specific device requires a persistent-current loop enclosing a remotely placed SQUID sensor. It may be possible to bond a thicker sensing-coil wire to thinner superconducting wires leading to a SQUID sensor, but it could be difficult to ensure reliable superconducting connections, especially if the bonded wires are made of different materials.



A Single-Turn Sensing Coil would be made by melting a low-melting-temperature superconducting metal onto a form encapsulating three insulated superconducting wires.

The proposed improvement would constitute a partial solution of some of the problems summarized above. The main idea is to mold the sensing coil in place, to more nearly optimum cross

sectional shape, instead of making the coil by winding standard prefabricated wire. For this purpose, a thin superconducting wire loop that is an essential part of the SQUID magnetometer would be encapsulated in a form that would serve as a mold. A low-melting-temperature superconducting metal (e.g., indium, tin, or a lead/tin alloy) would be melted into the form, which would be sized and shaped to impart

the required cross section to the coil thus formed. The figure depicts an example of a design incorporating the proposed improvement.

*This work was done by Konstantin Penanen, Inseob Hahn, and Byeong Ho Eom of Caltech for NASA's Jet Propulsion Laboratory. Further information is contained in a TSP (see page 1).*

*In accordance with Public Law 96-517, the contractor has elected to retain title to this inven-*

*tion. Inquiries concerning rights for its commercial use should be addressed to:*

*Innovative Technology Assets Management  
JPL*

*Mail Stop 202-233  
4800 Oak Grove Drive  
Pasadena, CA 91109-8099  
E-mail: iaoffice@jpl.nasa.gov*

*Refer to NPO-44397, volume and number of this NASA Tech Briefs issue, and the page number.*

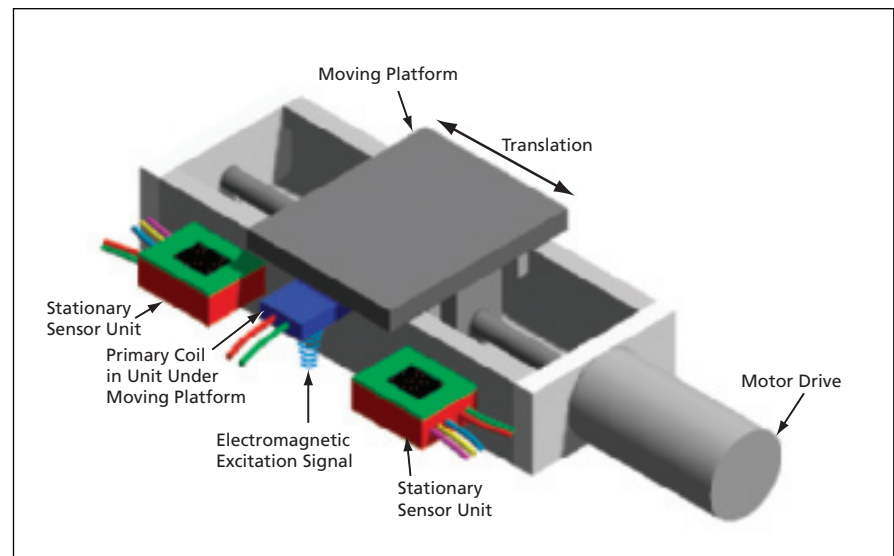
## Inductive Linear-Position Sensor/Limit-Sensor Units

**These non-contact devices afford more information than do mechanical limit switches.**

*Marshall Space Flight Center, Alabama*

A new sensor (see figure) provides an absolute position measurement. The figure presents a schematic view of a motorized linear-translation stage that contains, at each end, an electronic unit that functions as both (1) a non-contact sensor that measures the absolute position of the stage and (2) a non-contact equivalent of a limit switch that is tripped when the stage reaches the nominal limit position. The need for such an absolute linear position-sensor/limit-sensor unit arises in the case of a linear-translation stage that is part of a larger system in which the actual stopping position of the stage (relative to the nominal limit position) must be known. Because inertia inevitably causes the stage to run somewhat past the nominal limit position, tripping of a standard limit switch or other limit sensor does not provide the required indication of the actual stopping position. This innovative sensor unit operates on an electromagnetic-induction principle similar to that of linear variable differential transformers (LVDTs).

Depending upon the application, this sensor technology can provide absolute position in various forms and can easily be integrated into users' designs. The basic sensor utilizes only two active inexpensive components. The sensor can be placed on an adhesive surface, or could be buried inside or underneath the outer skin of a component. The sensor technology can be physi-



A Linear Translation Stage is equipped with linear-position-sensor/limit-sensor units.

cally scaled up or down and can even be employed inside a microelectromechanical-system (MEMS) device. The sensor can be designed with redundant sensor coils without additional physical volume.

In testing, the sensor produced accuracies of 4  $\mu\text{m}$ , and greater accuracies are possible with other sensor configurations. The sensor can use excitation frequencies ranging from several kilohertz to the megahertz region. The sensor is extremely repeatable with data correlations of 0.99999 or greater. This simple sensor technology has been

patented and is available for licensing opportunities.

*This work was done by Dean Alhorn, David Howard, and Dennis Smith of Marshall Space Flight Center and Kenneth Dutton of Sverdrup Technology, Inc. Further information is contained in a TSP (see page 1).*

*This invention has been patented by NASA (U.S. Patent No. 7,116,098). Inquiries concerning nonexclusive or exclusive license for its commercial development should be addressed to Sammy Nabors, MSFC Commercialization Assistance Lead, at sammy.a.nabors@nasa.gov. Refer to MFS-32192-1.*



## Hilbert-Curve Fractal Antenna With Radiation-Pattern Diversity

Two radiation patterns are attainable without active switching.

John H. Glenn Research Center, Cleveland, Ohio

A printed, folded, Hilbert-curve fractal microwave antenna has been designed and built to offer advantages of compactness and low mass, relative to other antennas designed for the same operating frequencies. The primary feature of the antenna is that it offers the advantage of radiation-pattern diversity without need for electrical or mechanical switching; it can radiate simultaneously in an end-fire pattern at a frequency of 2.3 GHz (which is in the S-band) and in a broadside pattern at a frequency of 16.8 GHz (which is in the Ku-band). This radiation-pattern diversity could be utilized, for example, in applications in which there were requirements for both S-band ground-to-ground communications and Ku-band ground-to-aircraft or ground-to-spacecraft communications. The lack of switching mechanisms or circuitry makes this antenna more reliable, easier, and less expensive to fabricate than it otherwise would be.

Fabrication of the antenna begins with etching of its Hilbert-curve fractal conductor pattern onto a single 5-mil (0.127-mm)-thick substrate of a dielectric material that has a relative permittivity ( $\epsilon_r$ ) of 2.2. The conductor is formed as a microstrip 0.5 mm wide. Notches are cut into the substrate to facilitate folding. Then the patterned, notched substrate is folded, along with 1-mm-thick separation layers made of a dielectric foam having  $\epsilon_r = 1.07$ , to form the multilayer structure shown in Figure 1. This multilayer structure is mounted onto an aluminum ground plane.

The antenna is excited via a probe feed. At 2.3 GHz, the antenna presents a matched reactive load to the probe feed and functions as a miniature dipolelike antenna that produces the end-fire radiation pattern [see Figure 2(a)]. The antenna can be tailored at this frequency by adjusting the length of the probe feed in conjunction with the location of the probe connection and by choice of strip-line width, strip-line spacings, and interlayer spacings. At frequencies in

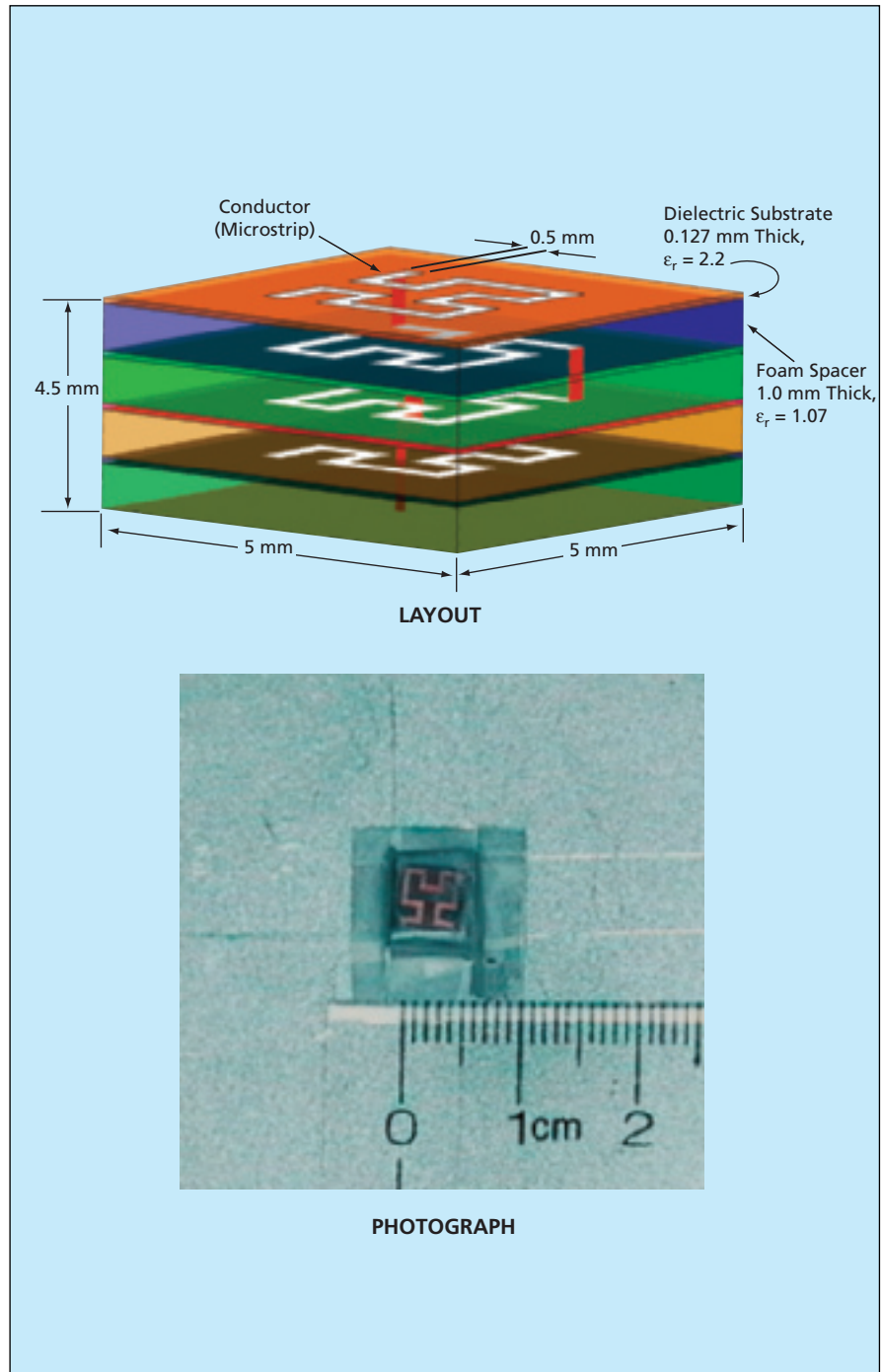


Figure 1. This **Multilayer Microstrip Antenna** radiates in an end-fire pattern (maximum gain in plane) at 2.3 GHz and in a broadside pattern (maximum gain perpendicular to plane) at 16.8 GHz. Dimensions shown here are typical and can be adjusted to optimize performance, change operating frequencies, or both.

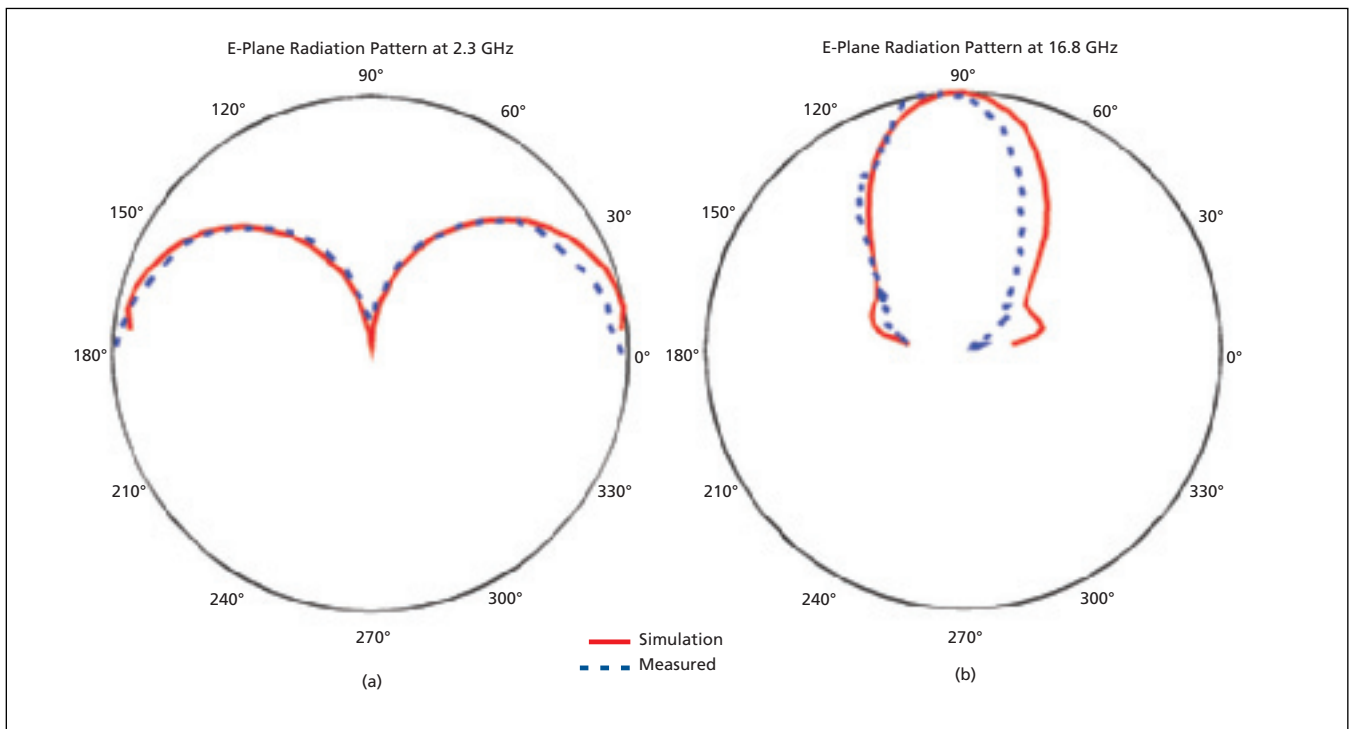


Figure 2. **Two Radiation Patterns** are attainable, as shown : (a) end-fire radiation pattern at 5-band and (b) broadside radiation pattern at Ku-band.

the vicinity of 16.8 GHz, the antenna resembles a square patch antenna having dimensions close to a half wavelength, resulting in a broadside radiation pattern characterized by gain and bandwidth comparable to those of a microstrip patch antenna designed for

operation in the same frequency range [see Figure 2(b)].

*This work was done by James A. Nessel, Félix A. Miranda, and Afroz Zaman of Glenn Research Center. Further information is contained in a TSP (see page 1).*

*Inquiries concerning rights for the commercial use of this invention should be addressed to NASA Glenn Research Center, Innovative Partnerships Office, Attn: Steve Fedor, Mail Stop 4-8, 21000 Brookpark Road, Cleveland, Ohio 44135. Refer to LEW-17927-1.*

## Single-Camera Panoramic-Imaging Systems

**It is not necessary to use multiple cameras covering narrower fields of view.**

*Marshall Space Flight Center, Alabama*

Panoramic detection systems (PDSs) are developmental video monitoring and image-data processing systems that, as their name indicates, acquire panoramic views. More specifically, a PDS acquires images from an approximately cylindrical field of view that surrounds an observation platform. In example of a major class of intended applications, a PDS mounted on top of a motor vehicle could be used to obtain unobstructed views of the surroundings (see Figure 1). In another such example, a PDS could be mounted above a roadway intersection for monitoring approaching and receding vehicles in order to provide image data on the vehicles as input to an automated traffic-control system. In either application, a running archive of the image



Figure 1. A **Prototype PDS Mounted on Top of a Car** acquired a panoramic image of the surroundings.

data acquired by the PDS could be maintained as a means of reconstructing the events leading up to a vehicular collision:

used in this way, a PDS would be analogous to an aircraft “black box” data recorder.

The main subsystems and components of a basic PDS are a charge-coupled-device (CCD) video camera and lens, transfer optics, a panoramic imaging optic, a mounting cylinder, and an image-data-processing computer. The panoramic imaging optic is what makes it possible for the single video camera to image the complete cylindrical field of view; in order to image the same scene without the benefit of the panoramic imaging optic, it would be necessary to use multiple conventional video cameras, which have relatively narrow fields of view.

The panoramic imaging optic can be any one of several different types of

wide-angle optics. Examples include a panoramic annular lens (PAL), a convex mirror, a fish-eye lens, scanning optics, or a panoramic refracting optic (PRO), which is described in the next paragraph. If necessary, the transfer optics can include one or more mirror(s) to flip the image. Downstream from the panoramic imaging optic and transfer optics, the image is further conditioned by the camera lens, then detected by the CCD in the camera. The camera output is digitized, processed by the computer, and displayed and/or stored as needed.

A PRO is a recently developed optic that operates partly like a PAL, partly like a fish-eye lens, and partly like a convex mirror. In comparison with a PAL, a PRO provides a wider field of view, yet is simpler and can be fabricated at lower cost. As shown in Figure 2, light from a scene enters the optic at location 1 (where it is refracted), travels through the optic, is totally internally reflected at location 2, leaves the optic at location 3 (where it undergoes a small amount of refraction), then goes through the transfer optics and camera lens into the camera. The net effect of refraction and reflection from surfaces of the optic is to define the wide, approximately cylindrical field of view. The limits of the field of view are deter-

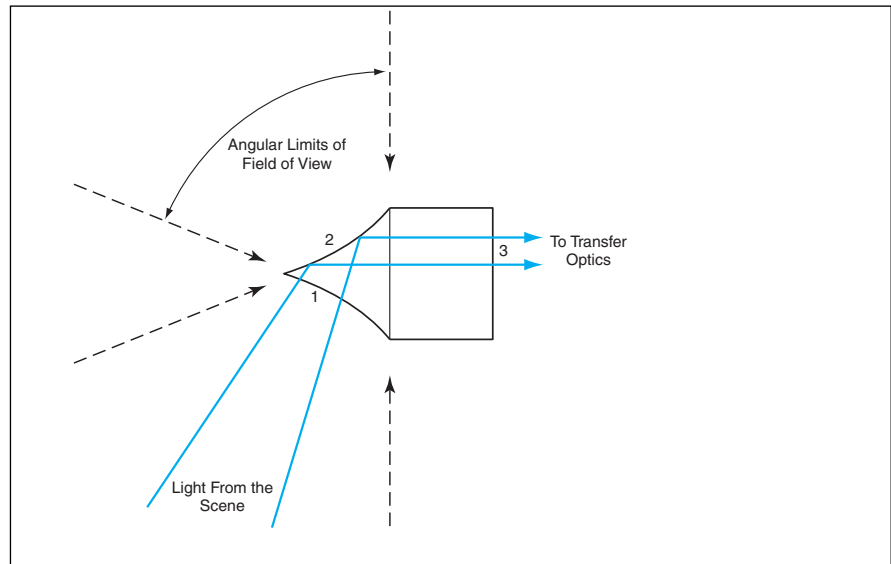


Figure 2. A Panoramic Refractive Optic utilizes both refraction and total internal reflection to enable projection from a wide, approximately cylindrical field of view onto a wide annulus in a focal plane.

mined primarily by the index of refraction of the optic and the curvature of its refracting/reflecting surface. A significant issue that remains to be addressed in subsequent development efforts is that the resolution of the image is approximately inversely proportional to the angular width of the field of view.

*This work was done by Jeffrey L. Lindner of Marshall Space Flight Center and John Gilbert of Optechnology, Inc. For*

*further information, contact Jim Dowdy, MSFC Commercialization Assistance Lead, at jim.dowdy@nasa.gov.*

*This invention has been patented by NASA (U.S. Patent No. 6,580,567). Inquiries concerning nonexclusive or exclusive license for its commercial development should be addressed to Sammy Nabors, MSFC Commercialization Assistance Lead, at sammy.a.nabors@nasa.gov. Refer to MFS-31432/75.*

## Interface Electronic Circuitry for an Electronic Tongue

**Compact, low-noise interface circuits are mounted in proximity to the tongue.**

*NASA's Jet Propulsion Laboratory, Pasadena, California*

Electronic circuitry has been developed to serve as an interface between an electronic tongue and digital input/output boards in a laptop computer that is used to control the tongue and process its readings. Electronic tongues were described in two prior *NASA Tech Briefs* articles: "Electronic Tongue for Quantitation of Contaminants in Water" (NPO-30601), Vol. 28, No. 2 (February 2004), page 31; and "Electronic Tongue Containing Redox and Conductivity Sensors" (NPO-30862), Vol. 31, No. 8 (August 2007), page 58. Electronic tongues can be used for a variety of purposes, including evaluating water quality, analyzing biochemicals, analyzing biofilms, and measuring electrical conductivities of soils.

The present electronic tongue and interface circuitry are updated versions of those described in the latter-mentioned

prior article. The instrument was designed for use in characterizing biofilms by Prof. D. Newman and Dr. D. Lies at Caltech. To recapitulate: An electronic tongue is a rugged, compact sensor unit that can include a heater, a temperature sensor, a conductivity sensor, and an array of three-electrode electrochemical cells, all on one planar surface of a ceramic substrate. The cells of an electronic tongue are connected to electronic excitation and readout circuits. Among the tasks identified by Prof. D. Newman and Dr. D. Lies that must be performed to characterize biofilms are stimulation of the microbial environment through generation of oxygen and hydrogen, detection of their metabolic products, and visual observation of biofilms. An electronic tongue can provide the needed stimulation while serving as a

means of electrochemical detection of metabolic products of a biofilm.

A prototype apparatus for characterizing a biofilm includes an electronic tongue mounted in a flow-through, see-into chamber. The chamber is mounted on a platform under a microscope that is used to observe the biofilm growing on the electronic tongue. The flow-through, see-into chamber is made of polycarbonate structural components plus a cover glass. A watertight compartment containing the electrodes is formed by O-ring seals between the upper and lower surfaces of the electronic tongue and the facing surfaces of the chamber. On the top side of the electronic tongue, a spacer establishes the thickness of the flow-through cell as a gap between the electrodes and the cover glass.

In the present version, the electronic tongue contains 12 analog cells: nine oxidation/reduction (redox) electrochemical cells, an electrical-conductivity cell, and the aforementioned heater and temperature sensor. The interface circuitry (see figure) consists mainly of 12 digital-to-analog converters (DACs) for excitation of the cells, and four analog-to-digital converters (ADCs) for readout from the cells connected to 12 analog cells. Each analog cell is made of two instrumental amplifiers, two operational amplifiers and analog filters for reduc-

ing signal-to-noise ratios, and control and switching circuits.

The interface circuitry resides on a board mounted immediately below the ceramic substrate and, as in the prior version, is connected to the analog cells via miniature edge connectors on the ceramic substrate. By thus placing the ADCs and DACs near the analog cells, the design helps to minimize pickup of noise and reduce cross-talk on the analog signal lines.

As in the prior version, the control circuitry can be programmed to make the DACs generate the specified excitation

waveforms and to make the ADCs acquire the specified response waveform data, and each electrochemical cell can be addressed individually. Depending on the specific application, a given electrochemical cell can be operated in a potentiostatic mode (voltage forced, current measured) or a galvanostatic mode (current forced, voltage measured), or can be made to alternate between the two modes. In one typical application, the main sequence of excitations and responses in a potentiostatic mode is chosen to implement anodic stripping voltammetry or cyclic voltammetry. In another typical application, a working electrode of a cell is operated in a galvanostatic mode at a positive bias for generating oxygen or a negative bias for generating hydrogen.

*This work was done by Didier Keymeulen and Martin Buehler of Caltech for NASA's Jet Propulsion Laboratory.*

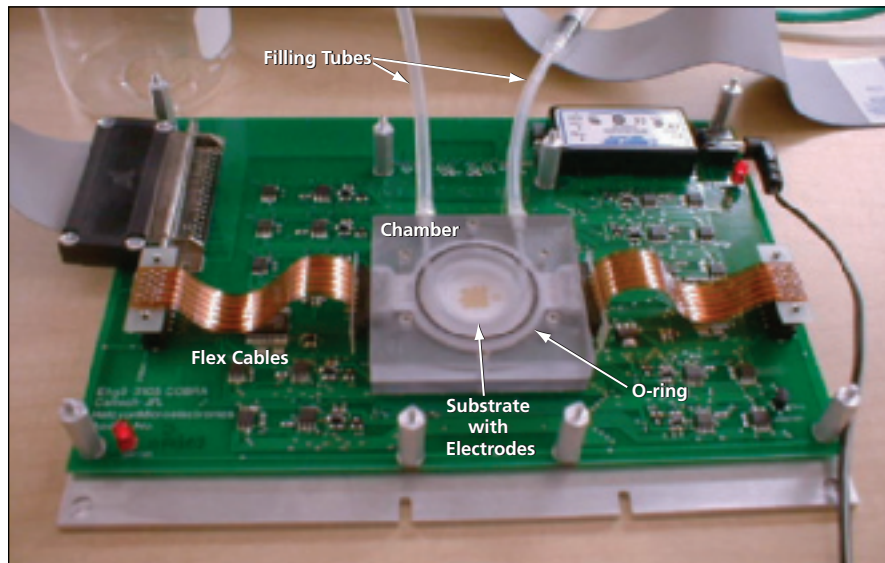
*In accordance with Public Law 96-517, the contractor has elected to retain title to this invention. Inquiries concerning rights for its commercial use should be addressed to:*

*Innovative Technology Assets Management  
JPL*

*Mail Stop 202-233  
4800 Oak Grove Drive  
Pasadena, CA 91109-8099  
(818) 354-2240*

*E-mail: iaoffice@jpl.nasa.gov*

*Refer to NPO-41365, volume and number of this NASA Tech Briefs issue, and the page number.*



The **Interface Circuitry** is laid out compactly on a board that, when installed, lies immediately below the electronic tongue.

## Inexpensive Clock for Displaying Planetary or Sidereal Time

**An external oscillator is substituted for an internal quartz clock oscillator.**

*NASA's Jet Propulsion Laboratory, Pasadena, California*

An inexpensive wall clock has been devised for displaying solar time or sidereal time as it would be perceived on a planet other than the Earth, or for displaying sidereal time on the Earth. The concept of a wall clock synchronized to a period other than the terrestrial mean solar day is not new in itself. What is new here is that the clock is realized through a relatively simple electronic modification of a common battery-powered, quartz-crystal-oscillator-driven wall clock (which, as unmodified, displays terrestrial mean solar time).

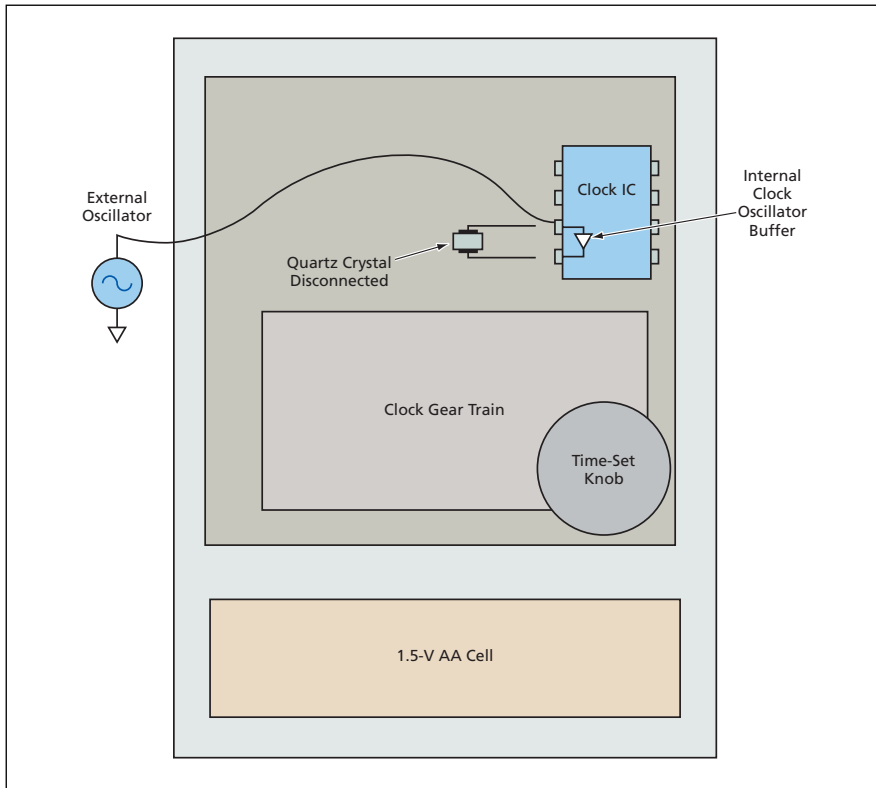
The essence of the modification is to shut off the internal oscillator of the clock and replace the internal-oscillator output signal with a signal of the required frequency generated by an external oscilla-

tor. The unmodified clock electronic circuitry includes a quartz crystal connected to an integrated circuit (IC) that includes, among other parts, a buffer amplifier that conditions the oscillator output. The modification is effected by removing the quartz crystal and connecting the output terminal of the external oscillator, via a capacitor, to the input terminal of the buffer amplifier (see figure).

The frequency and amplitude of the external-oscillator signal must be chosen in accordance with the IC design as well as the desired clock speed. Typically, the required amplitude is 0.5 V peak-to-peak and the frequency required for two complete revolutions of the hour hand (two 12-hour cycles) spanning a terrestrial mean solar day is  $2^{15} = 32,768$  Hz. Examples of other clock cycles

and frequencies based on this typical design include the following:

- For one complete revolution of the hour hand (one 24-hour cycle) during a terrestrial mean solar day, the required frequency is  $2^{14} = 16,384$  Hz.
- For two complete revolutions of the hour hand (two 12-“hour” cycles) during a terrestrial sidereal day, the required frequency is 32,859.27577 Hz.
- For one complete revolution of the hour hand (one 24-“hour” cycle) during a terrestrial sidereal day, the required frequency is 16,429.63788 Hz.
- For two complete revolutions of the hour hand (two 12-“hour” cycles) during a Martian mean solar day, the required frequency is 31,947.1361 Hz.
- For one complete revolution of the



An External Oscillator Is Substituted for the internal quartz-crystal oscillator of a common battery-powered wall clock.

hour hand (one 24-“hour” cycle) during a Martial sidereal day, the required frequency is 15,973.568 Hz.

It is worthwhile to note that for the 24-hour or for any of the 24-“hour” clock speeds, the minute hand would complete a revolution in 2 hours or “hours”. Therefore, it could be desirable to remove the minute hand to prevent confusion. In addition, in that case, the 12-hour faceplate must be replaced by a 24-hour faceplate.

It is also worthwhile to note that the precision of the clock display depends on the precision of the external oscillator, which can be cheap or expensive, as needed to obtain the precision required for a specific application. For example, the external oscillator could be a battery-powered, fixed-frequency quartz oscillator; a commercially available programmable integrated-circuit frequency synthesizer; or a programmable frequency synthesizer locked to highly stable reference oscillator (e.g., a hydrogen maser).

*This work was done by James Lux of Caltech for NASA’s Jet Propulsion Laboratory. Further information is contained in a TSP (see page 1). NPO-40845*

## Efficient Switching Arrangement for $(N + 1)/N$ Redundancy

This arrangement can be generalized beyond its initial application.

NASA’s Jet Propulsion Laboratory, Pasadena, California

An efficient arrangement of four switches has been conceived for coupling, to four output ports, the output powers of any subset of four devices that are members of a redundant set of five devices. In normal operation, the output power of each of four of the devices would be coupled to one of the four output ports. The remaining device would be kept as a spare: normally, its output power would be coupled to a load, wherein that power would be dissipated. In the event of failure of one of the four normally used devices, that device would be disconnected from its output port and connected to the load, and the spare device would be connected to the output from which the failed device was disconnected. Alternatively or in addition, the outputs of one or more devices could be sent to ports other than the ones originally assigned to them.

In the original intended application, the devices would be microwave amplifiers and the switches would be mechan-

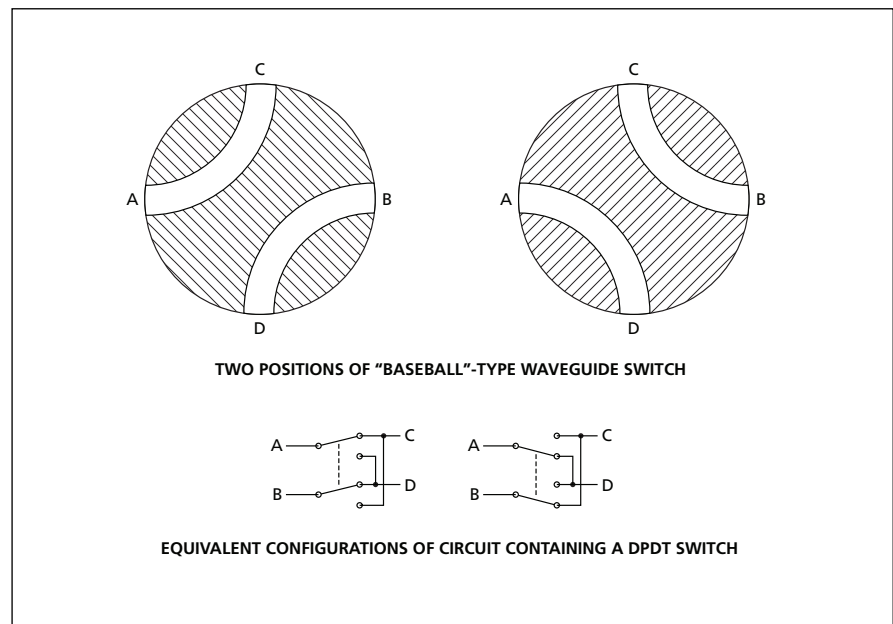


Figure 1. Ports A, B, C, and D can be connected in either of two different combinations of pairs, depending on the setting of a waveguide switch of the “baseball” type. Nominally equivalent switching could be effected by use of an electric circuit containing a DPDT switch.

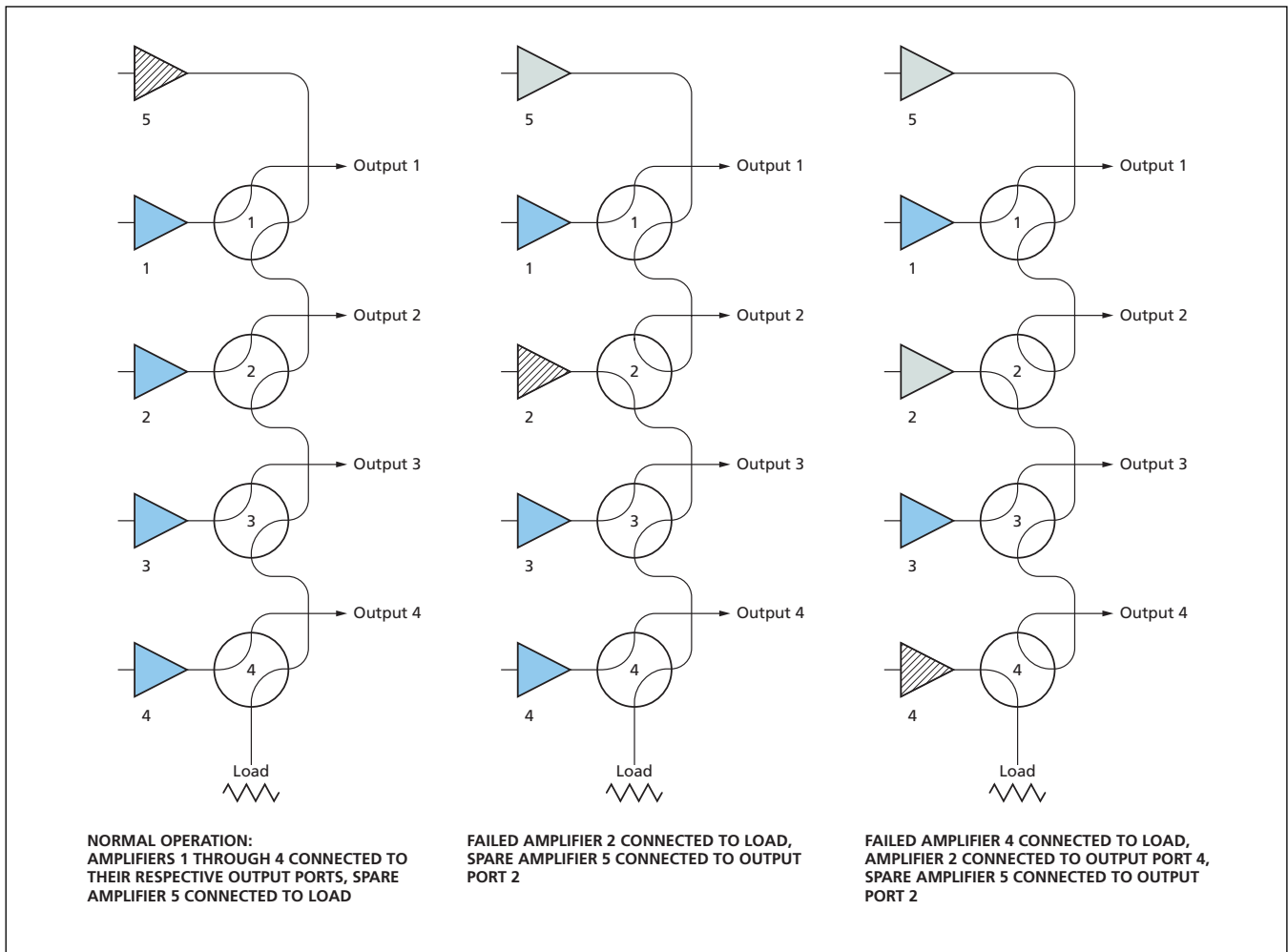


Figure 2. These **Three Switching Configurations** are a few examples of the larger number of allowable configurations for directing the outputs of four of the five amplifiers to the four output ports.

ically actuated waveguide switches. The arrangement could also be generalized to devices other than microwave amplifiers, to switches other than mechanically actuated microwave switches, and to greater numbers of switches, ports, and devices ( $N$ ,  $N$ , and  $N + 1$ , respectively, where  $N > 4$ ).

The mechanically actuated microwave switches in the original application would be two-position, four-port switches of a type known in the art as “baseball switches” because of the resemblance between their

waveguide cross sections and the patterns of stitches on baseballs. Figure 1 depicts the two positions of a baseball switch and the corresponding positions of a nominally equivalent circuit containing a double-pole, double-throw (DPDT) switch.

Figure 2 depicts three examples of useable switching configurations representative of the modes of operation described above. It should be apparent from casual inspection that any of those modes can be attained by actuation of one or more switches. In the original ap-

plication and perhaps in other potential applications, safety considerations dictate that switching configurations be limited to those in which every amplifier is connected to either an output port or to the load; non-connection of an amplifier or connection of an amplifier to another amplifier is not allowed.

*This work was done by James Lux and Robert McMaster of Caltech for NASA’s Jet Propulsion Laboratory. Further information is contained in a TSP (see page 1). NPO-41421*

## **Lightweight Reflectarray Antenna for 7.115 and 32 GHz**

**Reflectarrays for two different frequency bands share the same aperture.**

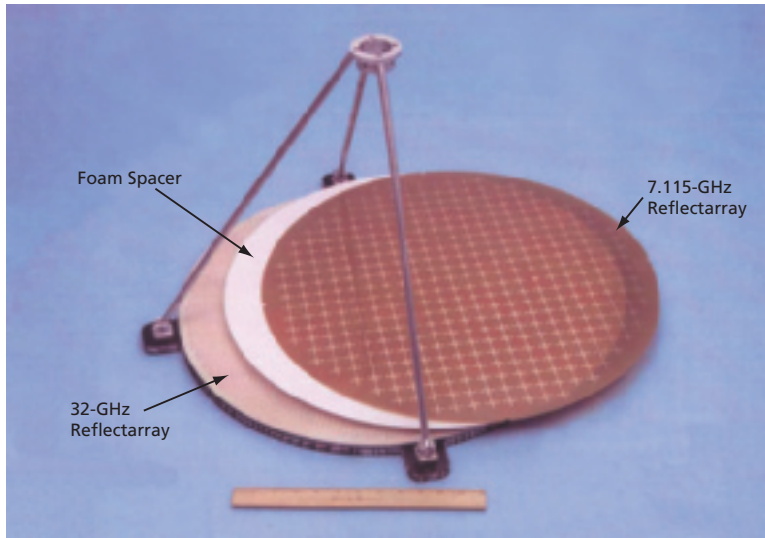
*NASA’s Jet Propulsion Laboratory, Pasadena, California*

A lightweight reflectarray antenna that would enable simultaneous operation at frequencies near 7.115 GHz and frequencies near 32 GHz is undergoing development. More precisely,

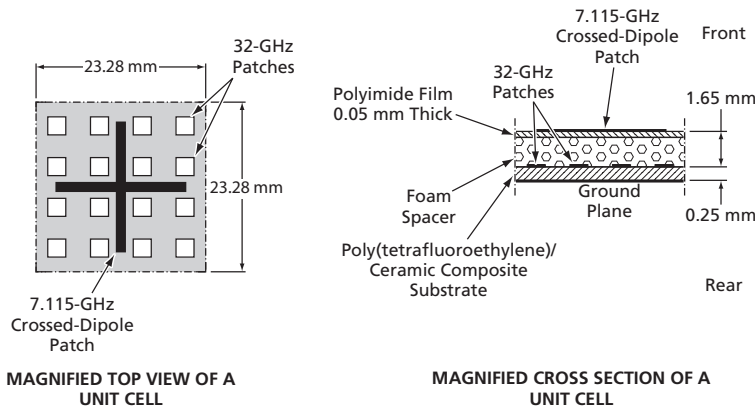
what is being developed is a combination of two reflectarray antennas — one for each frequency band — that share the same aperture. (A single reflectarray cannot work in both frequency

bands.) The main advantage of the single dual-band reflectarray is that it would weigh less and occupy less space than do two single-band reflectarray antennas.





PHOTOGRAPH SHOWING DUAL-BAND REFLECTARRAY ANTENNA PARTLY DISASSEMBLED



Two Reflectarrays for Different Frequency Bands are sandwiched together with a dielectric foam spacer to form a single dual-band reflectarray.

A reflectarray antenna consists mainly of a planar array of microstrip patches on a suitable dielectric substrate. In a prototype of the dual-band reflectarray antenna (see figure), the 7.115-GHz reflectarray antenna consists of crossed dipole microstrip patches on a thin polyimide membrane; the 32-GHz reflectarray antenna consists of square microstrip patches on top and a ground plane on the bottom of a poly(tetrafluoroethylene)/ceramic composite substrate. The ground plane is bonded to a supporting aluminum plate. The 7.115-GHz reflectarray is placed in front, and the two reflectarrays are sandwiched together with a dielectric foam spacer between them. The crossed-dipole patches of the front (7.115-GHz) reflectarray are positioned between the square patches of the rear (32-GHz) reflectarray to minimize blockage of radiation from the rear array.

In tests of the prototype antenna, it was found that the front (7.115-GHz reflectarray) caused a 1.8-dB reduction in the 32-GHz gain, while the effect of the rear (32-GHz) reflectarray on the 7.115-GHz performance was negligible. It was also concluded, on the basis of the test data, that there is a need to refine understanding of interactions between the individual reflectarrays and to refine their designs accordingly.

*This work was done by Mark Zawadzki and John Huang of Caltech for NASA's Jet Propulsion Laboratory. Further information is contained in a TSP (see page 1). NPO-40689*

## Opto-Electronic Oscillator Using Suppressed Phase Modulation

Phase noise would be much lower than in prior OEOs.

NASA's Jet Propulsion Laboratory, Pasadena, California

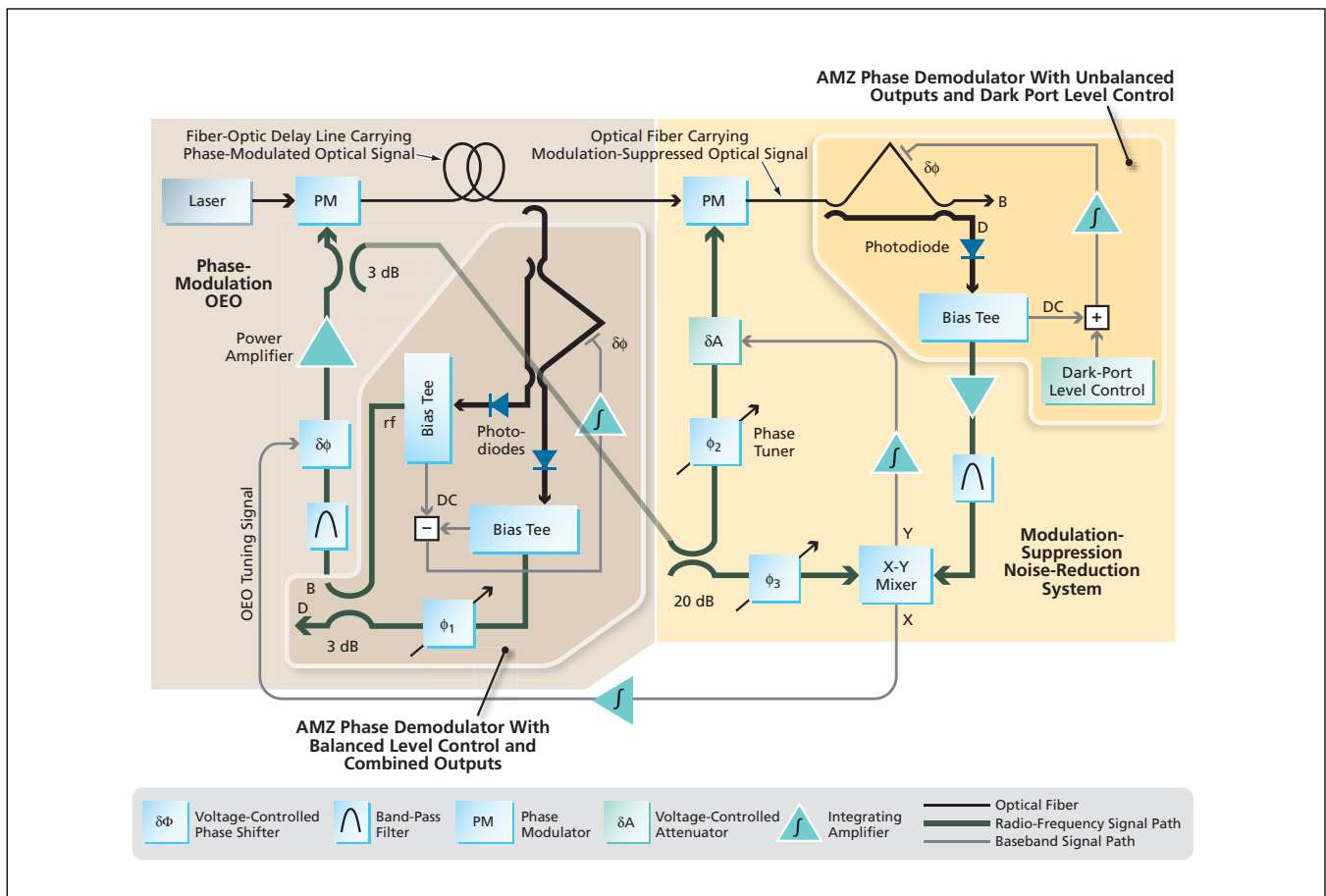
A proposed opto-electronic oscillator (OEO) would generate a microwave signal having degrees of frequency stability and spectral purity greater than those achieved in prior OEOs. The design of this system provides for reduction of noise levels (including the level of phase noise in the final output microwave signal) to below some of the fundamental limits of the prior OEOs while retaining the advantages of photonic generation of microwaves. Whereas prior OEOs utilize optical amplitude modulation, this system would utilize a combination of optical phase modulation and suppression

thereof. The design promises to afford, in the opto-electronic domain, the low-noise advantages of suppression of carrier signals in all-electronic microwave oscillators.

OEOs that utilize suppression of radio-frequency carrier signals have already been demonstrated to reject amplifier flicker noise. However, a second important advantage of microwave carrier suppression — reduction of the effects of thermal noise or shot noise (photon-counting noise) — has not previously been realized in OEOs. In microwave applications, realization of this

advantage is made possible by (1) use, in oscillators or interferometers, of power levels higher than can be tolerated by a low-noise follower amplifier, combined with (2) means for reducing power levels at detectors while preserving sensitivity. In the proposed system, realization of this advantage would be made possible by notable aspects of the design that would enable the use of high optical power levels to reduce shot-noise-induced variation in the frequency of an OEO.

The proposed system (see figure) would include two subsystems: a phase-



This **Modulation-Suppressed OEO** would generate a microwave signal having a degree of spectral purity higher than those of prior OEOs.

modulation OEO and a modulation-suppression noise-reduction subsystem. Each subsystem would contain an asymmetric Mach-Zehnder (AMZ) phase demodulator, which would be a combination of an AMZ interferometer with voltage-controlled phase tuning in one arm, and a photodiode at either or both of two optical output ports. The length differential between the two arms is approximately matched to one half of the wavelength of the radio-frequency (RF) modulation signal, typically 1.5 cm for an X-band (10-GHz) modulation signal. With appropriate choice of delays and of phase shifts ( $\phi_1$ ,  $\phi_2$ ,  $\phi_3$ ), the AMZ in the modulation-suppression noise-reduction

system would couple almost all of the optical power to a termination at one of its output ports, denoted the bright port and labeled “B” in the figure. The small remaining portion of the optical power, in the form a suppressed-carrier signal, would be coupled to a low-noise photodiode at the other port, denoted the dark port and labeled “D” in the figure. This arrangement would afford high sensitivity, at the photodiode output, to input phase modulation.

Sideband amplitude would also be reduced before detection by use of a phase “un-modulator” — a second phase modulator, at the output end of the fiber-optic delay line, that would exert an approxima-

tion of the reverse of the effect of the phase modulator at the input end of the line. Thus, both the carrier and the sideband components of the optical signal arriving at the low-noise photodiode in the AMZ phase demodulator in the modulation-suppression noise-reduction subsystem would be suppressed, thereby helping to prevent overload of the low-noise photodiode as optical power is increased. (Prevention of overload is necessary for preservation of sensitivity because low-noise photodiodes saturate at low optical power levels.)

*This work was done by G. John Dick and Nan Yu of Caltech for NASA’s Jet Propulsion Laboratory. For further information, contact [iaoffice@jpl.nasa.gov](mailto:iaoffice@jpl.nasa.gov). NPO-42815*

## Alternative Controller for a Fiber-Optic Switch

**This controller communicates via a serial instead of a parallel port.**

*NASA’s Jet Propulsion Laboratory, Pasadena, California*

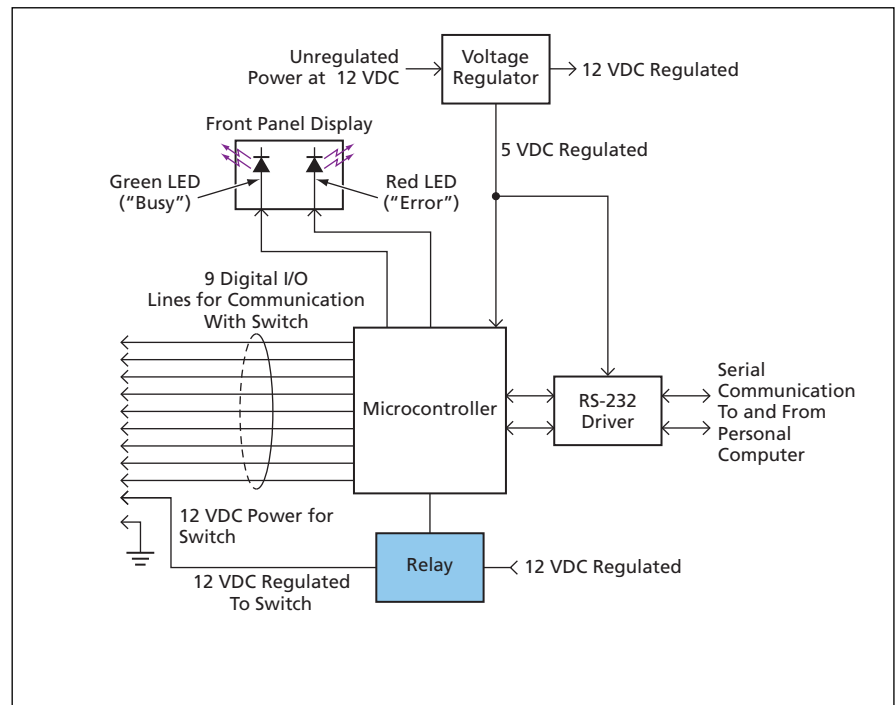
The figure is a simplified diagram of a relatively inexpensive controller for a DiCon VX (or equivalent) fiber-optic switch — an electromechanically actu-

ated switch for optically connecting one or two input optical fibers to any of a number of output optical fibers. DiCon VX fiber-optic switches are used prima-

rily in research and development in the telecommunication industry. This controller can control any such switch having up to 32 output channels.

A digital input/output (I/O) interface circuit is needed for controlling the switch and reading its status. This controller was developed as an alternative to the control interface suggested by the manufacturer of the switch. The manufacturer provides a schematic diagram of an interface circuit that utilizes the parallel port of a personal computer, and provides sample software for use with the interface. However, the parallel ports on some personal computers are not compatible with the interface suggested by the manufacturer. In contrast, the present controller uses a standard RS-232 serial interface, which is available on most computers and can ordinarily be utilized with less difficulty than can a personal-computer parallel port.

The heart of this controller is a commercially available microcontroller that includes 16 digital I/O ports and flash memory that can hold up to 1KB of program. The controller also includes an RS-232 driver. Two of the digital I/O lines are used for serial communication, via the RS-232 driver, between the microcontroller and the personal computer. Nine of the digital I/O lines are used for controlling the switch and reading its status. One of the digital I/O lines is used to control the power to the switch through a relay, and two of these lines are used to drive a two-color light-emitting-diode (LED) front-panel display. The software enables a user to interactively control the switch by means of simple commands and to monitor the re-



This **Controller for a Fiber-Optic Switch** is an alternative to a more-difficult-to-use controller that communicates with a computer via a parallel interface.

sponses of the switch. The front-panel display enables the user to determine the status of the switch (“busy” or “error”) at a glance.

The serial-port architecture of this controller facilitates establishment of an interface between this controller and commercially available laboratory automation software. It is also possible to connect this controller to a universal se-

rial port via an appropriate converter. Therefore, the switch can be controlled by a variety of computers, without need for expensive digital I/O boards or complicated programming.

*This work was done by Robert Peters of Caltech for NASA’s Jet Propulsion Laboratory. Further information is contained in a TSP (see page 1). NPO-43306*





## Strong, Lightweight, Porous Materials

**These materials, derived from silica aerogels, can be tailored to have superior properties.**

*John H. Glenn Research Center, Cleveland, Ohio*

A new class of strong, lightweight, porous materials has been invented as an outgrowth of an effort to develop reinforced silica aerogels. The new material, called X-Aerogel is less hygroscopic, but no less porous and of similar density to the corresponding unmodified aerogels. However, the property that sets X-Aerogels apart is their mechanical strength, which can be as much as two and a half orders of magnitude stronger than the unmodified aerogels. X-Aerogels are envisioned to be useful for making extremely lightweight, thermally insulating, structural components, but they may also have applications as electrical insulators, components of laminates, catalyst supports, templates for electrode materials, fuel-cell components, and filter membranes.

In broad terms, X-Aerogels are formed by chemical reaction of a cross-linking agent with the surfaces of the nanoporous network of the native aerogel. The cross-linking agent may be a monomeric or an oligomeric precursor of a polymer that forms a conformal

coating on the nanoparticles, reinforcing the underlying structure while preserving the mesoporosity. The nanoporous network itself may consist of silica, alumina, titania, vanadia, or other metal oxide aerogels. Research with various other oxide nanoparticle skeletal frameworks has led to X-Aerogels based on approximately 35 different metals from the Periodic Table.

The nanoparticles that comprise the aerogels can be cross-linked in their native form through the hydroxyl groups, which are found naturally on their surface. Thus, the first class of X-Aerogels utilizes isocyanates for cross-linking, which react both with the surface hydroxyl groups and any water adsorbed on the surfaces of the nanoparticles. This limits polymer accumulation only on the internal surfaces of the aerogel, leaving the mesopores empty. The result is a greatly reinforced structure at a minimal increase in density.

While the isocyanate cross-linked aerogels show great improvements in properties, relying on the native hy-

droxyl group functionality of aerogels for cross-linking limits the variety of possible precursors that can react with the mesoporous surfaces. This issue has been addressed by chemical modification of the aerogel itself. The mesoporous surface of silica has been modified with amines and olefins, and the resulting particles have been cross-linked with epoxides and with polystyrene. Many other combinations of surface functional groups and cross linkers can be envisioned, which would impart additional desired properties to the X-Aerogels.

*This work was done by Nicholas Leventis, Mary Ann B. Meador, and James C. Johnston of Glenn Research Center and Eve F. Fabrizio and Ulvi Ilhan of Ohio Aerospace Institute. Further information is contained in a TSP (see page 1).*

*Inquiries concerning rights for the commercial use of this invention should be addressed to NASA Glenn Research Center, Innovative Partnerships Office, Attn: Steve Fedor, Mail Stop 4-8, 21000 Brookpark Road, Cleveland, Ohio 44135. Refer to LEW-17685-1.*

## Nanowicks

**Fiber geometries could be tailored for pumping, filtering, mixing, separating, and other effects.**

*NASA's Jet Propulsion Laboratory, Pasadena, California*

Nanowicks are dense mats of nanoscale fibers that are expected to enable the development of a variety of novel capillary pumps, filters, and fluidic control devices. Nanowicks make it possible to obtain a variety of novel effects, including capillary pressures orders of magnitude greater than those afforded by microscale and conventional macroscale wicks. While wicking serves the key purpose of transporting fluid, the nanofiber geometry of a nanowick makes it possible to exploit additional effects — most notably, efficient nanoscale mixing, fluidic effects for logic or control, and ultrafiltration (in which mats of nanofibers act as biomolecular sieves).

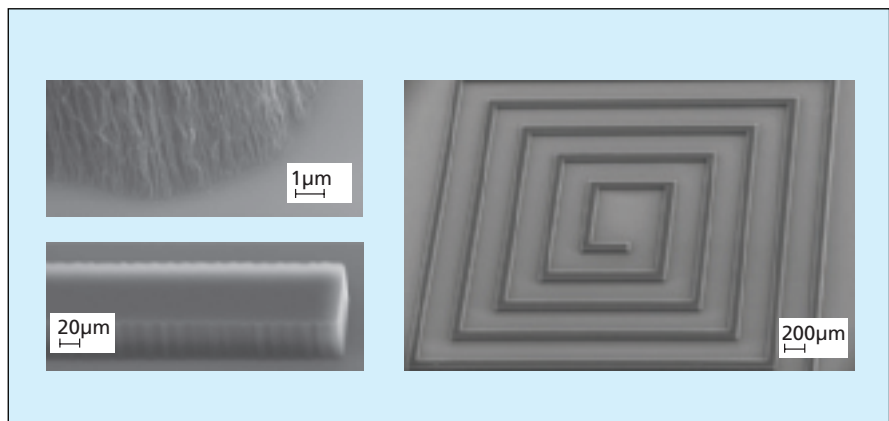


Figure 1. This Scanning Electron Micrograph depicts a nanowick in the form of a mat of carbon nanotubes, which can be grown in a tailorable pattern as shown on the right.

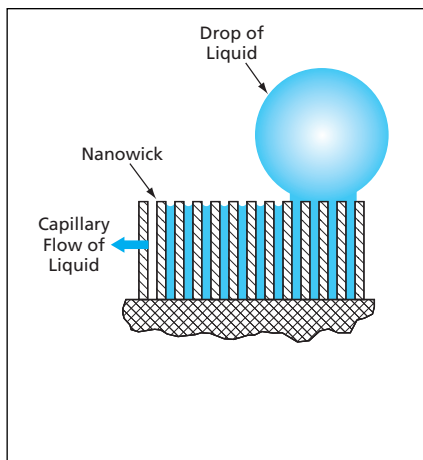


Figure 2. A Drop of Liquid would be placed on a nanowick. The liquid would be absorbed into the wick and transported by capillary action.

A nanowick (see Figure 1) typically consists of carbon nanotubes grown normal to a substrate in a tailorable pattern. The liquid of interest is constrained to flow in the interstices between the fibers. (In practice, the liquid must include a surfactant because carbon nanotubes are hydrophobic.) By suitable control of the growth process, the interfiber distance and/or the fiber length can be made to range from nanometers to millimeters and to vary with position (in one or two dimensions) on the substrate. Similarly, the fiber diameter can be made to vary with position. The spatial variation in spacing and/or diameter can be chosen to obtain such effects as prescribed spatial variations in wicking speed or pre-

scribed degrees of separation among different biomolecules.

The following are examples of potential applications and potential variations in designs of nanowicks:

- Somewhat analogously to strips of litmus paper, wicking chips could be made as disposable devices for rapid testing of liquids. To start a test, a drop of liquid would be placed on top of the array of nanofibers on a wicking chip (see Figure 2). After absorption of the drop and transport of the liquid by wicking, the liquid could be filtered and analyzed (for viscosity, for example) in a very simple manner, without need for any complicated pumping mechanism.
- A liquid could be made to flow continuously, as in a capillary-pumped loop. The liquid would enter a nanowick at one end, would flow through the mat of fibers by capillary action, and would be made to evaporate at the other end. The evaporation would sustain the pumping action in the same manner in which evaporation of water from leaves sustains capillary pumping in living plants.
- A nanowick could serve as both a filter and a pump: While a liquid was flowing through a nanowick, the fibers could trap particles and large molecules (for example, protein and deoxyribonucleic acid molecules).
- The pattern of nanofibers could be tailored to exploit a combination of diffusion and extensional flow to promote nanoscale mixing of two liquids.
- Nanowicks could be patterned to act as

various fluidic logic devices, including ones that exert fluidic effects analogous to the electrical effects of transistors and diodes. Unlike macroscale and microscale fluidic devices, the nanowick-based fluidic devices could, conceivably, be designed and built without channels and could operate without mechanical pumps.

- It might be possible to construct nanowicks in which selective wicking could be controlled electrically.
- Although capillary forces would suffice to contain a liquid within a nanowick, without need to place the wick in a channel, the nanowick could be capped, if desired, to prevent evaporation.
- Nanowicks could be used to transport liquids through interstitial spaces into which tubes could not be inserted.

*This work was done by Flavio Noca, Michael Bronikowski, Elijah Sansom, Jijie Zhou, and Morteza Gharib of Caltech for NASA's Jet Propulsion Laboratory. Further information is contained in a TSP (see page 1).*

*In accordance with Public Law 96-517, the contractor has elected to retain title to this invention. Inquiries concerning rights for its commercial use should be addressed to:*

*Innovative Technology Assets Management  
JPL*

*Mail Stop 202-233  
4800 Oak Grove Drive  
Pasadena, CA 91109-8099  
(818) 354-2240*

*E-mail: iaoffice@jpl.nasa.gov  
Refer to NPO-40440, volume and number of this NASA Tech Briefs issue, and the page number.*

## Lightweight Thermal Protection System for Atmospheric Entry

The material withstands up to 1,970 K to protect wing leading edges and nose caps on hypersonic vehicles.

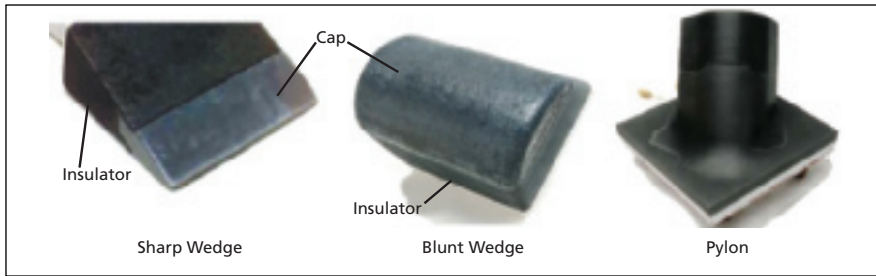
Ames Research Center, Moffett Field, California

TUFROC (Toughened Uni-piece Fibrous Reinforced Oxidation-resistant Composite) has been developed as a new thermal protection system (TPS) material for wing leading edge and nose cap applications. The composite withstands temperatures up to 1,970 K, and consists of a toughened, high-temperature surface cap and a low-thermal-conductivity base, and is applicable to both sharp and blunt leading edge vehicles. This extends the possible application of fibrous insulation to the wing leading edge and/or nose cap on a hypersonic vehicle.

The lightweight system comprises a treated carbonaceous cap composed of ROCCI (Refractory Oxidation-resistant Ceramic Carbon Insulation), which provides dimensional stability to the outer mold line, while the fibrous base material provides maximum thermal insulation for the vehicle structure. The composite has graded surface treatments applied by impregnation to both the cap and base. These treatments enable it to survive in an aero-convectively heated environment of high-speed planetary entry. The exact cap and base materials are chosen in combination with the surface treatments,

taking into account the duration of exposure and expected surface temperatures for the particular application.

Current leading edge TPS systems weigh approximately 1.6 g/cm<sup>3</sup>, while the TUFROC version weighs 0.4 g/cm<sup>3</sup>. The RCC system used on the orbiter operates at heat fluxes below 70 W/cm<sup>2</sup> during Earth re-entry. Not only are systems like this heavier than TUFROC, they are far more expensive with RCC costing approximately 100 times more than TUFROC components of equivalent size. Furthermore, RCC requires significantly longer fabrication lead times — 12 rather than the



Various Configurations of TUFROC have been prepared and tested in high-energy arc-jet environments.

roughly a month needed for TUFROC. TUFROC systems have been fabricated and tested in the various configurations as shown in the figure. The 5° blunt cone is 6.35 cm thick, and has a 1.27 cm corner radius. The sharp leading edge wedge has a 10° half-angle, is 10.2 cm wide, and has leading edge radii

of 0.158 cm and 0.318 cm. The blunt leading edge wedge has a leading edge radius of 5.08 cm and is 20.2 cm wide. These configurations have thermocouples installed at the junction between the cap and insulator, and in the aluminum base-plate behind the insulation. Finally, to evaluate the flight perform-

ance of a TUFROC TPS on the wing leading edge of the X-37, a pylon test article was created consisting of two tiles: a base tile (20.3×20.3 cm square) with a pylon protruding from it, and an upper portion 10.2 cm long. All test articles, except the pylon, contain a threaded aluminum-mounting ring bonded into their bases so that they can be attached to a water-cooled strut.

*This work was done by David Stewart and Daniel Leiser of NASA's Ames Research Center. Further information is contained in a TSP (see page 1).*

*This invention is owned by NASA, and a patent application has been filed. Inquiries concerning rights for the commercial use of this invention should be addressed to the Ames Technology Partnerships Division at (650) 604-2954. Refer to ARC-15201-1.*







## Rapid and Quiet Drill

This is an all-ultrasonic variant of previously reported ultrasonic/sonic drills.

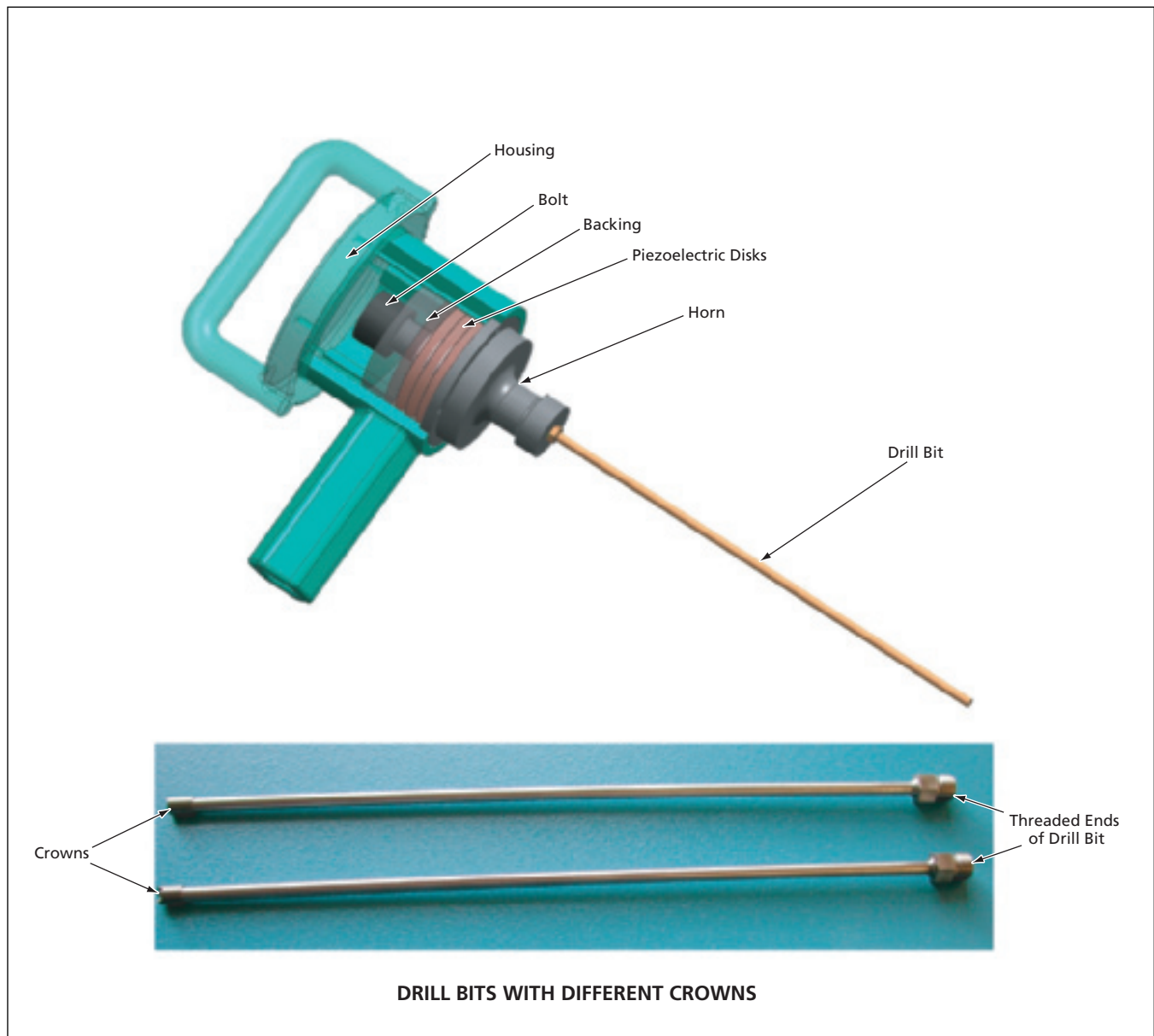
NASA's Jet Propulsion Laboratory, Pasadena, California

The figure depicts selected aspects of the rapid and quiet drill (RAQD), which is a prototype apparatus for drilling concrete or bricks. The design and basic principle of operation of the RAQD overlap, in several respects, with those of ultrasonic/sonic drilling and coring apparatuses described in a number of

previous *NASA Tech Briefs* articles. The main difference is that whereas the actuation scheme of the prior apparatuses is partly ultrasonic and partly sonic, the actuation scheme of the RAQD is purely ultrasonic. Hence, even though the RAQD generates considerable sound, it is characterized as quiet because most or all of

the sound is above the frequency range of human hearing.

The ultrasonic transducer in the RAQD consists of a stack of piezoelectric disks, their electrodes, and a backing layer, all held in compression by a bolt that also holds them in place on a horn. During operation, the piezoelectric stack



The **Rapid and Quiet Drill** is designed to make little or no audible sound while penetrating concrete. Because drill bits are thread-mounted, they can be changed in the field.

is driven at a frequency of 24.8 kHz. A drill bit is attached to the horn by means of a simple threaded connection: for this purpose, the proximal end of the drill bit is threaded and widened, and the thread on the drill bit matches the thread in a hole on the tip of the horn. The drill bit is tipped with a crown having a cutting edge (which could be toothed) chosen to

suit the specific application. The crown is attached to the bolt by brazing and, hence, can be replaced when it is worn out. The bolt, horn, drill bit, and crown are all hollow so that, optionally, air can be blown through them to remove dust from the drilled hole.

*This work was done by Stewart Sheritt, Mircea Badescu, Yoseph Bar-Cohen, Zensheu*

*Chang, and Xiaoqi Bao of Caltech for NASA's Jet Propulsion Laboratory.*

*This invention is owned by NASA, and a patent application has been filed. Inquiries concerning nonexclusive or exclusive license for its commercial development should be addressed to the Patent Counsel, NASA Management Office-JPL. Refer to NPO-42131.*

## Hydrogen Peroxide Concentrator

Water is removed through selectively permeable membranes.

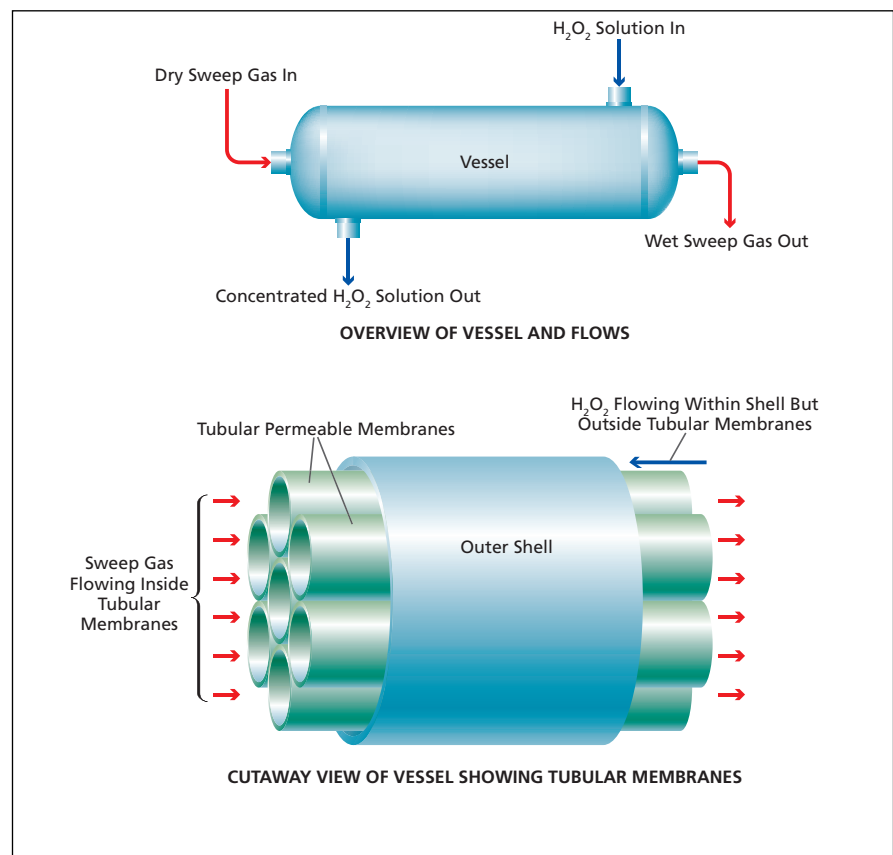
*John F. Kennedy Space Center, Florida*

A relatively simple and economical process and apparatus for concentrating hydrogen peroxide from aqueous solution at the point of use have been invented. The need for this or a similar invention arises for the following reasons:

- The highest commercial grade of hydrogen peroxide has a concentration of 70 volume percent.
- Concentrations of more than 80 volume percent are required in some industrial and some military propulsion applications.
- Prior methods of concentration of hydrogen peroxide are expensive and can entail production of quantities larger than can be utilized immediately. The necessity of storing and handling the excess concentrated hydrogen peroxide poses a safety problem.

The heart of the apparatus is a vessel (see figure) comprising an outer shell containing tubular membranes made of a polymer that is significantly more permeable by water than by hydrogen peroxide. The aqueous solution of hydrogen peroxide to be concentrated is fed through the interstitial spaces between the tubular membranes. An initially dry sweep gas is pumped through the interiors of the tubular membranes. Water diffuses through the membranes and is carried away as water vapor mixed into the sweep gas. Because of the removal of water, the hydrogen peroxide solution flowing from the vessel at the outlet end is more concentrated than that fed into the vessel at the inlet end.

The concentration process as described thus far would ordinarily and preferably be run in a continuous, counter-flow mode. Optionally, it could be run in a batch mode. The rate of removal of water can be increased by increasing the rate of flow of the sweep gas. Also, the water capacity of the sweep gas and, hence, the rate of removal of



An **Aqueous Hydrogen Peroxide Solution** flows within the outer shell, in the interstices between the tubular membranes. Water diffuses from the solution into the interiors of the membranes, where the flowing sweep gas carries it away.

water can be increased by heating the sweep gas, taking care to keep the temperature less than the lower of either (1) the boiling point of the hydrogen peroxide solution, (2) the temperature above which the hydrogen peroxide decomposes spontaneously, or (3) the maximum temperature that the membrane can endure without deteriorating. The sweep gas can be air, nitrogen, or any other gas that can be conveniently supplied in dry form and does not react chem-

ically with hydrogen peroxide.

The selections of the membrane, outer-shell, and plumbing materials are governed largely by the following criteria:

- All of the affected materials should be chemically nonreactive with hydrogen peroxide at the highest concentration expected to be encountered.
- The membrane material should be capable of sustaining a high flux of

water so that the total membrane area needed to sustain a given rate of removal of water can be made as small as possible.

- The selectivity of the membrane, here defined as ratio between its permeability by water and its permeability by hydrogen peroxide, should preferably be greater than 2.

Suitable membrane materials include

polysulfone and perfluorinated polymers having sulfonic or carboxylic ionic functional groups.

The viability of the invention has been demonstrated in tests. For example, in one test in which the membrane material was a perfluorosulfonic polymer, the sweep gas was air at ambient atmospheric pressure, and the temperature was 42 °C, a 69.6-percent hydrogen peroxide solu-

tion was concentrated to 85.4 percent in 80-percent yield.

*This work was done by Clyde F. Parrish of Kennedy Space Center.*

*This invention has been patented by NASA (U.S. Patent No. 7,122,166). Inquiries concerning nonexclusive or exclusive license for its commercial development should be addressed to the Kennedy Innovative Partnerships Office at (321) 861-7158. Refer to KSC-12666.*





## MMIC Amplifiers for 90 to 130 GHz

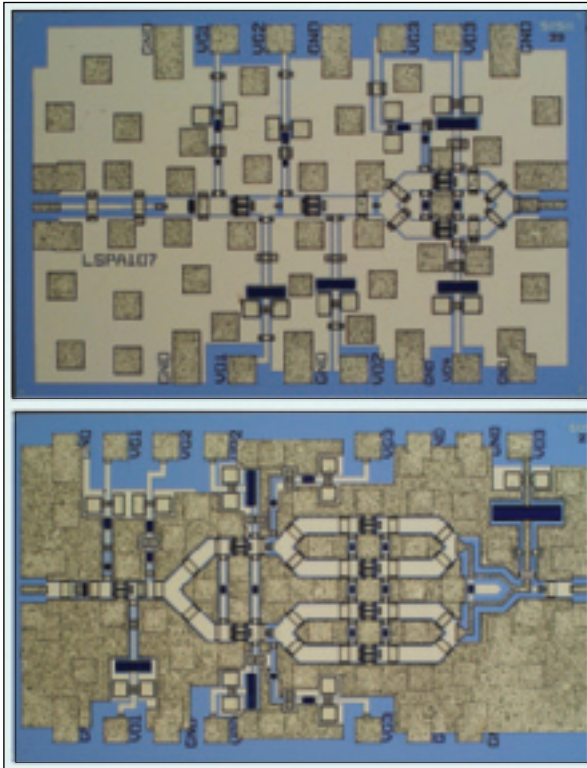
Output power exceeds that of prior solid-state amplifiers operating above 110 GHz.

NASA's Jet Propulsion Laboratory, Pasadena, California

The figure shows two monolithic microwave integrated-circuit (MMIC) amplifier chips optimized to function in the frequency range of 90 to 130 GHz, covering nearly all of E-band (90 – 140 GHz). These amplifiers were designed specifically for local-oscillator units in astronomical radio telescopes such as the Atacama Large Millimeter Array (ALMA). They could also be readily adapted for use in electronic test equipment, automotive radar systems, and communications systems that operate between 90 and 130 GHz.

There have been many published articles about MMIC power-amplifier chips and modules that operate at lower frequencies in W-band (75–110 GHz). Such chips typically provide 50 to 300 mW of output power per 0.6 to 1.2 mm of gate periphery of the transistors on the chips, and contain either GaAs or InP high-electron-mobility transistors (HEMTs) or InP heterojunction bipolar transistors. The radio-frequency interconnections on such chips have been primarily made with microstrip transmission lines, which are particularly convenient for large eight-way power-combining networks. For higher frequencies, it may be more beneficial to use grounded coplanar waveguide transmission lines to avoid the added source inductances required in microstrip circuits to provide grounds for the transistors. The present 90–130 GHz MMIC amplifiers are products of an effort to increase the operating frequency of power amplifiers beyond W-band utilizing co-planar waveguide circuitry, while also increasing the number of transistors to be power-combined on a chip (and hence, the maximum output power).

One of the challenges in designing MMIC power amplifiers to operate above W-band is the choice of transistor.



These MMIC Amplifier Chips operate in the frequency range of 90 to 130 GHz. The final stage of the chip shown at the top contains a two-way power combiner; the final stage of the chip shown at the bottom contains a four-way power combiner.

InP HEMTs having gate lengths no larger than 0.12  $\mu\text{m}$  are the most mature technology available, though InP double-heterojunction bipolar transistors are starting to gain ground. A second challenge is to power-combine as many large-periphery transistors as possible within the constraints of matching networks at the higher frequencies. The best W-band power amplifiers utilize eight-way power combiners for a total gate periphery of 1.2 mm. Since power-combining field-effect transistors (FETs) involves placing source vias between the FETs, the compactness of power-combining structures becomes more difficult as wavelength decreases. One result of the constraints imposed by design rules, fabrication processes, and current-carrying capacities of the transmission line circuit elements, is that the range of coplanar-

waveguide impedances available for matching networks is restricted approximately to between 23 and 65  $\Omega$ .

The present two MMIC amplifier chips were designed with these challenges and constraints in mind. The transistors on these chips are 0.11- $\mu\text{m}$ -gate-length AlInAs/GaInAs/InP HEMT devices grown by molecular-beam epitaxy at HRL Laboratories, LLC. These transistors exhibit typical DC transconductances of 1,050 mS/mm and breakdown voltages of 4 V. The transistors include four gate fingers, each 37  $\mu\text{m}$  wide, making a total periphery of 148  $\mu\text{m}$ . The circuitry is formed using a grounded coplanar-waveguide transmission lines on a 50- $\mu\text{m}$ -thick InP substrate. Vias between the top ground planes and back-side metal are used to suppress unwanted substrate waveguide modes. The chip shown in the upper part of the figure incorporates three stages. The final stage contains two power-combined HEMTs, so that the total gate periphery of the output stage is about 300  $\mu\text{m}$ . The chip shown in the lower part of the figure incorporates three stages. The final stage on this chip contains a four-way power combiner at the output; hence, the total gate periphery of the output stage of this chip is about 600  $\mu\text{m}$ . The amplifier chips were mounted in waveguide modules. When tested, these amplifier modules exhibited gains of 15 to 20 dB and output powers from 20 to 45 mW — the highest output powers thus far obtained from any solid-state amplifier modules above 110 GHz.

*This work was done by Lorene Samoska, David Pukala, and Alejandro Peralta of Caltech for NASA's Jet Propulsion Laboratory; Eric Bryerton, Matt Morgan, and T. Boyd of the National Radio Astronomy Observatory; and Ming Hu and Adele Schmitz of HRL Laboratories, LLC. Further information is contained in a TSP (see page 1). NPO-41481*





### Robot Would Climb Steep Terrain

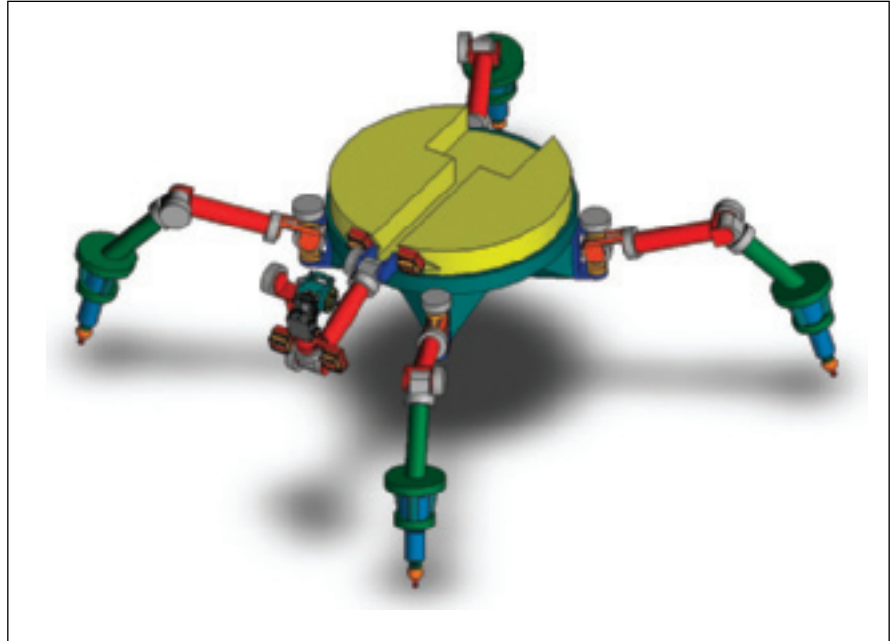
**This walking robot could even climb under overhangs.**

*NASA's Jet Propulsion Laboratory, Pasadena, California*

The figure depicts the steep terrain access robot (STAR) — a walking robot that has been proposed for exploring steep terrain on remote planets. Robots based on the STAR concept could also be used on steep terrain on Earth for diverse purposes that could include not only scientific exploration but also military reconnaissance and search-and-rescue operations.

The STAR would be able to climb up or down on slopes as steep as vertical, and even beyond vertical to overhangs. Its system of walking mechanisms and controls would be to react forces and maintain stability. The STAR would be capable of performing such tasks as acquisition of samples and placement of instruments. To enable the STAR to anchor itself in the terrain on steep slopes to maintain stability and react forces, it would be necessary to equip the tips of the walking legs with new ultrasonic/sonic drill corers (USDCs) and to develop sensors and control algorithms to enable robust utilization of the USDCs.

The plan for the initial stage of development calls for construction of a prototype STAR as a combination of a walking robot, denoted the LEMUR IIb, that was described in "Modification of a Legged Robot to Favor Climbing" (NPO-40354), *NASA Tech Briefs*, Vol. 30, No. 4 (April 2006), page 80. The prototype would enable testing of



The **Steep Terrain Access Robot** would walk by use of legs tipped with ultrasonic/sonic devices that would anchor themselves in the terrain.

the STAR concept on planar slopes. Eventually, a robot more like the one shown in the figure would be constructed. This robot would be capable of moving over slopes having three-dimensional features.

*This work was done by Brett Kennedy, Anthony Ganino, Hrand Aghazarian, Robert Hogg, Michael McHenry, and Michael Gar-*

*rett of Caltech for NASA's Jet Propulsion Laboratory. Further information is contained in a TSP (see page 1).*

*The software used in this innovation is available for commercial licensing. Please contact Karina Edmonds of the California Institute of Technology at (626) 395-2322. Refer to NPO-41158.*

### Measuring Dynamic Transfer Functions of Cavitating Pumps

**Flow and pressure perturbations are imposed; transfer functions are computed from responses.**

*Marshall Space Flight Center, Alabama*

A water-flow test facility has been built to enable measurement of dynamic transfer functions (DTFs) of cavitating pumps and of inducers in such pumps. Originally, the facility was intended for use in an investigation of the effects of cavitation in a rocket-engine low-pressure oxygen turbopump. The facility can also be used to measure DTFs of cavitating pumps in general.

It is necessary to measure DTFs in order to understand the dynamic couplings between a cavitating pump and the rest of the flow system of which the pump is a part. In the case of a turbopump, inducer cavitation dynamics can cause flow and pressure pulsations arriving at the turbopump inlet to become amplified by the turbopump, thereby giving rise to very large flow

and pressure fluctuations in the feed system served by the turbopump. If the feed system in question is a rocket-engine fuel or oxidizer feed system, these flow and pressure fluctuations can, in turn, cause large variations in engine thrust, even to the point of pogo instability. Within the turbopump, the cavitation-induced dynamic couplings generate intense dynamic loads on the

inducer blades and the rotor. These loads cause blade failures, seal rubs, and rotordynamic instabilities.

The DTF-measurement facility was constructed by integrating DTF-measuring equipment into a prior pump-testing facility. The major pieces of the DTF-measuring equipment, in order of position along the flow starting at the upstream end, are an inlet flow pulser, inlet flow conditioner, inlet bandwidth-enhanced electromagnetic flowmeter, inlet pressure-measurement station, test inducer, discharge collector, exit flow conditioner, exit enhanced-bandwidth electromagnetic flowmeter, exit flow pulser, flow conditioner, loop flowmeter, and

throttle valve. A magnetic-bearing-supported test rotor that was part of the original pump-testing facility is used to support and drive the test inducer. A closed reservoir from the original pump-testing facility is retained for supplying fluid to the inlet and receiving fluid from the outlet of the pump or inducer under test. The facility also includes instrumentation and data-acquisition and data-processing systems designed specifically for quantifying dynamic transfer functions of cavitating inducers.

The flow pulsers can be used to superimpose discrete-frequency pressure and flow fluctuations on the mean loop flow. The enhanced-bandwidth electromag-

netic flowmeters enable accurate measurement of the time-dependent components of flow. Special-purpose software calculates parameters of a four-terminal transfer function model of the cavitating pump or inducer system from the amplitudes and relative phases of inlet and exit flow and pressure pulsations over a range of perturbation frequencies and cavitation numbers.

*This work was done by Daniel Baun of Concepts NREC for Marshall Space Flight Center. For further information, contact Sammy Nabors, MSFC Commercialization Assistance Lead, at [sammy.a.nabors@nasa.gov](mailto:sammy.a.nabors@nasa.gov). Refer to MFS-32519-1.*





## Advanced Resistive Exercise Device

**A number of different exercises can be performed on one machine.**

*Lyndon B. Johnson Space Center, Houston, Texas*

The advanced resistive exercise device (ARED), now at the prototype stage of development, is a versatile machine that can be used to perform different customized exercises for which, heretofore, it has been necessary to use different machines. Conceived as a means of helping astronauts and others to maintain muscle and bone strength and endurance in low-gravity environments, the ARED could also prove advantageous in terrestrial settings (e.g., health clubs and military training facilities) in which many users are exercising simultaneously and there is heavy demand for use of exercise machines.

The ARED is a fairly simple, robust machine. It is designed to enable the user to perform the three primary resistive exercises, for stimulating bone regeneration and exercising the major muscle groups. It also has the ability to perform 15 other exercises for secondary muscle groups. For the original low-gravity application, it is required to simulate the lifting of weights in normal Earth gravitation, and to have an operational life of 15 years. The major sub-

systems of the ARED are a pair of vacuum cylinders, a frame-and-platform assembly, an arm base assembly, a wishbone arm/lift bar, a cable-and-pulley mechanism, and a flywheel mechanism:

- The frame-and-platform assembly serves as a backbone that supports all other subsystems and components.
- The vacuum cylinders provide constant resistance for exercise. These are commercial off-the-shelf pneumatic cylinders of 8 in. ( $\approx 20$  cm) inside diameter. If necessary, the cylinders can be recharged by use of a vacuum source. The vacuum cylinders are connected to the frame-and-platform assembly and the arm base assembly.
- The arm base assembly serves as a load-adjustment mechanism and is a part of the overall load path.
- The wishbone arm/lift bar serves as the bar exercise interface for the user, enabling the user to perform the squat, dead lift, heel raise, and many other exercises. The wishbone arm is also in the direct load path from the arm base assembly to the user.

- The cable-and-pulley mechanism is connected to the arm base assembly. It is designed primarily to enable the user to perform long-stroke, low-load exercises. Examples of cable-and-pulley exercises are arm flies and hip abductions.
- The flywheel mechanism provides the equivalent of the inertial component of free-weight exercise. This mechanism includes a gear rack that is attached to a piston shaft and meshes with a gear train connected to a flywheel. When this mechanism is in use, movement of the lift bar causes rotation of the flywheel.

*This work was done by Jasen Raboin, Jason Niebuhr, Santana Cruz, and Chris Lamoreaux of Johnson Space Center. For further information, contact the Johnson Innovative Partnerships Office at (281) 483-3809.*

*This invention is owned by NASA, and a patent application has been filed. Inquiries concerning nonexclusive or exclusive license for its commercial development should be addressed to the Patent Counsel, Johnson Space Center, (281) 483-0837. Refer to MSC-23805.*

## Rapid Engineering of Three-Dimensional, Multicellular Tissues With Polymeric Scaffolds

**Engineered tissues could be grown in weeks or days instead of months.**

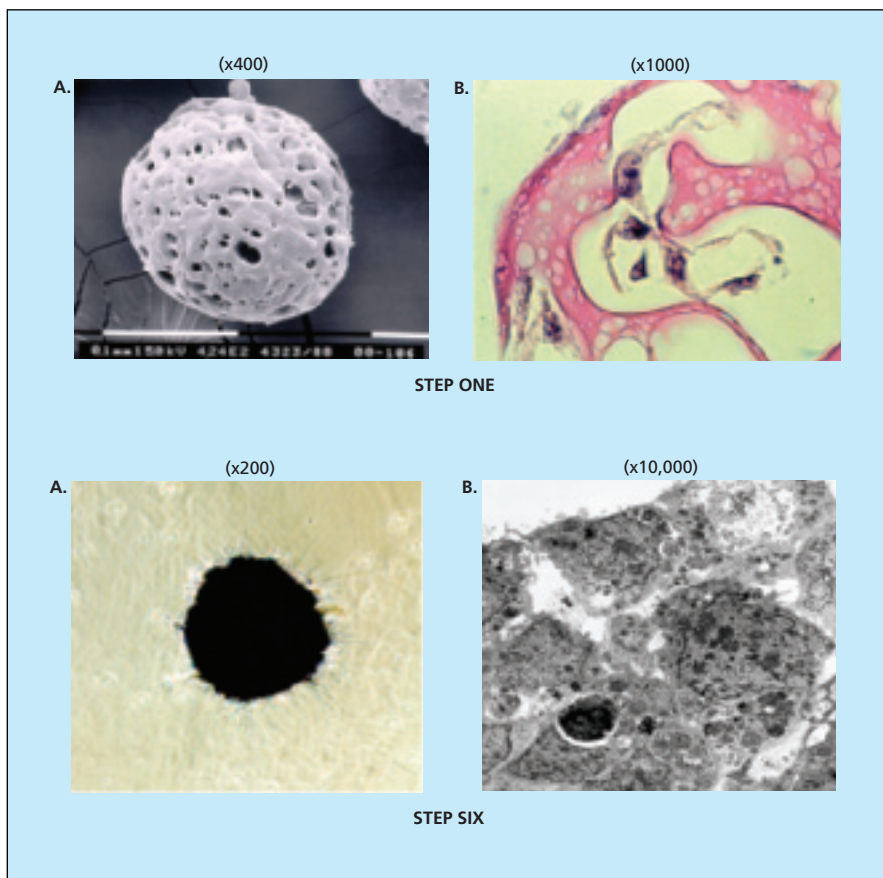
*Lyndon B. Johnson Space Center, Houston, Texas*

A process has been developed for the rapid tissue engineering of multicellular-tissue-equivalent assemblies by the controlled enzymatic degradation of polymeric beads in a low-fluid-shear bioreactor. In this process, the porous polymeric beads serve as temporary scaffolds to support the assemblies of cells in a tissue-like 3D configuration during the critical initial growth phases of attachment of anchorage-dependent cells, aggregation of the cells, and formation of a 3D extracellular matrix. Once the cells are assembled into a 3D array and enmeshed in a structural sup-

portive 3D extracellular matrix (ECM), the polymeric scaffolds can be degraded in the low-fluid-shear environment of the NASA-designed bioreactor. The natural 3D tissue-like assembly, devoid of any artificial support structure, is maintained in the low-shear bioreactor environment by the newly formed natural cellular/ECM. The elimination of the artificial scaffold allows normal tissue structure and function.

The advantages afforded by the enzymatic-digestion method, relative to the prior method, arise in connection with much greater speed of digestion. The

biodegradable polymers commonly used heretofore as scaffolding materials have been poly(lactic acid), poly(glycolic acid), and copolymers of lactic and glycolic acids. The time needed for complete degradation of scaffolding made from these polymers typically ranges from 10 to 52 weeks, the exact time depending on the chemical composition of the polymer. Such long degradation times are problematic, especially when 3D tissue assemblies without artificial materials are needed in much shorter times (for example, for growth of autologous tissue to be im-



**Twelve Porous Beads** were used as scaffolds to grow multicellular spheroids, which, when enzymatically digested in a low-shear bioreactor, resulted in 3D tissuelike assemblies.

planted to replace damaged or diseased tissue). In contrast, the enzymatic-degradation method enables complete digestion of polymeric scaffolding within days.

For a tissue-engineering process that incorporates this enzymatic-digestion process, one must select a scaffolding material amenable to enzymatic degradation. For an experiment in which such

a process was demonstrated, dextran-based beads were selected as the scaffolding and dispase (a neutral protease) was selected as an enzyme that could digest the beads without damaging cell membranes or disrupting the 3D tissuelike infrastructure. The beads were initially incubated with rat fibroblasts for four days on a rotary shaker, then the fibroblast-coated beads (see upper part of figure) were inoculated into a nutrient fluid in a horizontal-axis rotating-vessel (HARV) bioreactor, which provided a low-shear flow environment. After one day of incubation in the HARV, human epithelial cells were inoculated and cultured for three days to allow the formation of a natural structural infrastructure comprising fibroblast-epithelial cell layers and a prominent ECM. Next, dispase was introduced into the culture medium to digest the beads and incubation was continued for another week. Microscopic examination of spheroids showed (see lower part of figure) that the controlled enzymatic degradation of an artificial matrix in the low shear environment of the NASA-designed bioreactor could rapidly produce 3D tissuelike spheroids free of any artificial infrastructure.

*This work was done by Steve R. Gonda of Johnson Space Center, Jacqueline Jordan of Universities Space Research Association, and Denise N. Fraga of Enterprise Advisory Service, Inc. For further information, contact the Johnson Innovative Partnerships Office at (281) 483-3809. MSC-23359*



## Resonant Tunneling Spin Pump

Electrons in opposite spin states would flow in opposite directions across a spin filter.

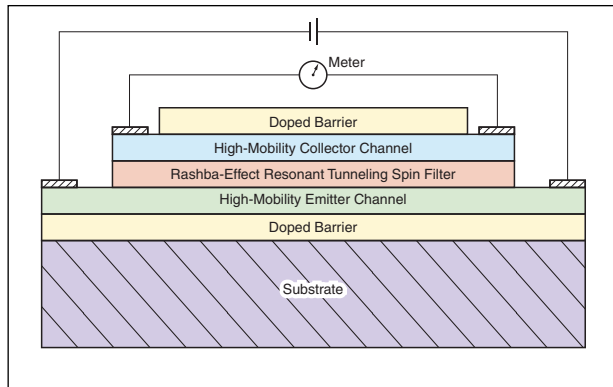
NASA's Jet Propulsion Laboratory, Pasadena, California

The resonant tunneling spin pump is a proposed semiconductor device that would generate spin-polarized electron currents. The resonant tunneling spin pump would be a purely electrical device in the sense that it would not contain any magnetic material and would not rely on an applied magnetic field. Also, unlike prior sources of spin-polarized electron currents, the proposed device would not depend on a source of circularly polarized light.

The resonant tunneling spin pump would have some features in common with other, similarly named devices, including resonant tunneling spin filters described in a previous NASA Tech Briefs article: "Electron-Spin Filters Based on the Rashba Effect" (NPO-30635), Vol. 28, No. 10 (October 2004), page 58.

To recapitulate: Proposed semiconductor electron-spin filters would exploit the Rashba effect, which can induce energy splitting in what would otherwise be degenerate quantum states, caused by a spin-orbit interaction in conjunction with a structural-inversion asymmetry in the presence of interfacial electric fields in a

semiconductor heterostructure. The magnitude of the energy split is proportional to the electron wave number. Theoretical studies have suggested the possibility of devices in which electron energy states would be split by the Rashba effect and spin-polarized currents would be extracted by resonant quantum-mechanical tunneling.



In the Resonant Tunneling Spin Pump, the lateral electric field applied to the emitter channel would induce a lateral current in the collector channel and spin-polarized currents across the spin filter.

The resonant tunneling spin pump (see figure) would include a spin filter between two reservoirs of initially unpolarized electrons. Like the devices of the cited prior article, the resonant tunneling spin pump would be designed and fabri-

cated in the InAs/GaSb/AlSb material system. One reservoir would be a high-mobility InAs emitter channel and the other a high-mobility InAs collector channel. The spin filter would comprise an InAs/GaSb/AlSb asymmetric resonant tunneling structure.

The application of a lateral electric field in the emitter channel would cause current of one spin state to flow from the emitter channel to the collector channel and a current of the opposite spin state to flow from the collector channel to the emitter channel, thereby inducing spin polarization in both reservoirs. This mode of operation would differ somewhat from that of a spin filter: In a spin filter, component currents containing spins of both states would flow from the emitter to the collector and spin polarization in the collector would be achieved by choosing the design and the operating conditions of the device to make one of the spin component currents larger than the other.

This work was done by David Z. Ting of Caltech for NASA's Jet Propulsion Laboratory. Further information is contained in a TSP (see page 1). NPO-30885

## Enhancing Spin Filters by Use of Bulk Inversion Asymmetry

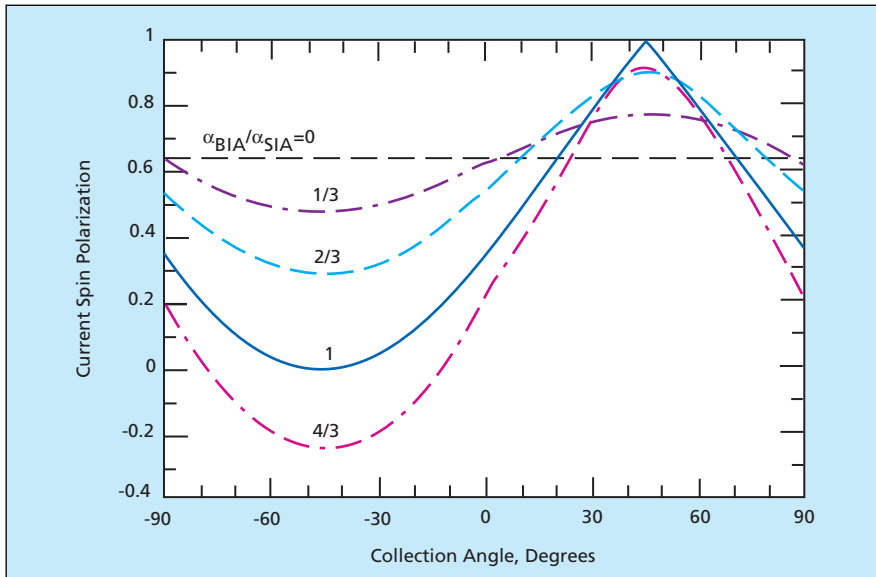
Current spin polarization could be maximized through appropriate choice of collection angle.

NASA's Jet Propulsion Laboratory, Pasadena, California

Theoretical calculations have shown that the degrees of spin polarization in proposed nonmagnetic semiconductor resonant tunneling spin filters could be increased through exploitation of bulk inversion asymmetry (BIA). These enhancements would be effected through suitable orientation of spin collectors (or spin-polarization-inducing lateral electric fields), as described below.

Spin filters — more precisely, sources of spin-polarized electron currents — have been sought for research on, and development of, the emerging technological discipline of spintronics (spin-transport electronics). Proposed nonmagnetic semiconductor electron-spin filters were described in a prior NASA Tech Briefs article: "Electron-Spin Filters Based on the Rashba Effect" (NPO-30635), Vol. 28, No. 10 (October 2004),

page 58. To recapitulate: The proposed spin filters were to be based on the Rashba effect, which is an energy splitting of what would otherwise be degenerate quantum states, caused by a spin-orbit interaction in conjunction with a structural-inversion asymmetry (SIA) in the presence of interfacial electric fields in a semiconductor heterostructure. The magnitude of the energy split is proportional to the electron wave num-



**Current Spin Polarization** was computed as a function of collection angle for different values of the ratio between the BIA and SIA coefficients ( $\alpha_{\text{BIA}}/\alpha_{\text{SIA}}$ ), under the simplifying assumption of perfect sub-band filtering.

ber. In a spin filter, the spin-polarized currents produced by the Rashba effect would be extracted by quantum-mechanical resonant tunneling.

The origin of the enhancement now proposed lies in recognition that not only

the SIA but also bulk inversion asymmetry (BIA) contributes to the spin-dependent energy splitting. The conceptual device structure on which the proposal is based is a spin-filtering resonant tunneling heterostructure, grown along the [001] direc-

tion (the z axis), that includes an asymmetric quantum well. The physics of this structure was represented by a simplified two-band, spin-dependent Hamiltonian model. This model was chosen because although it is only approximate, its simplicity facilitates understanding of how BIA could be utilized to enhance spin filtering.

The theoretical calculations were performed using this model. It was found that when only SIA is taken into account, the theoretical upper limit of current spin polarization for a Rashba-effect resonant tunneling spin filter with a one-sided spin collector can be expected to be  $2/\pi$  (about 63.7 percent), independent of the direction of the collector. When BIA was taken into account along with SIA, it was found that current spin polarization could be changed from the SIA-only value by varying the collection angle: in particular, the greatest and least polarization values were found to occur in the [110] and  $[1\bar{1}0]$  directions, representing collection angles of  $+45^\circ$  and  $-45^\circ$ , respectively.

*This work was done by David Ting and Xavier Cartoixa of Caltech for NASA's Jet Propulsion Laboratory. For more information, contact iaoffice@jpl.nasa.gov. NPO-40210*

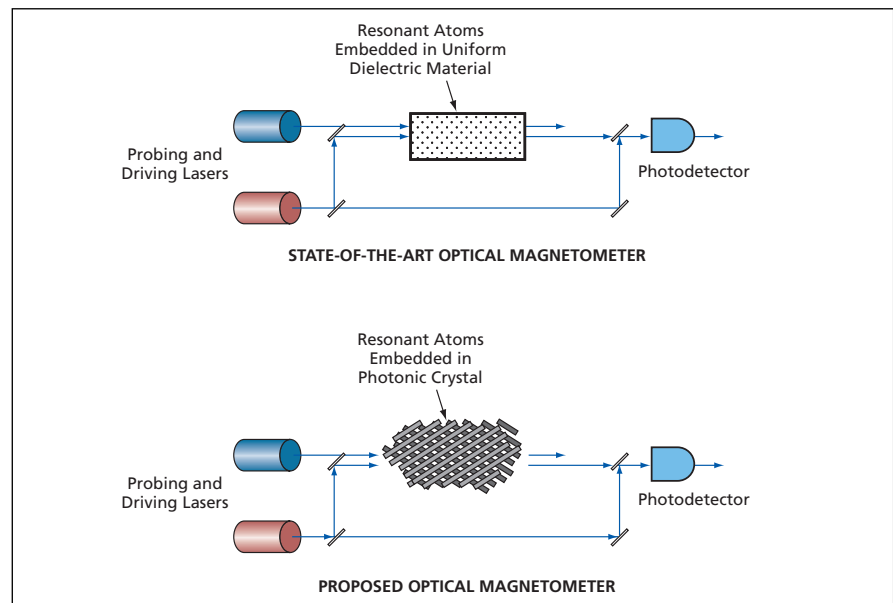
## Optical Magnetometer Incorporating Photonic Crystals

Sensitivity would be increased by orders of magnitude.

NASA's Jet Propulsion Laboratory, Pasadena, California

According to a proposal, photonic crystals would be used to greatly increase the sensitivities of optical magnetometers that are already regarded as ultrasensitive. The proposal applies, more specifically, to a state-of-the-art type of quantum coherent magnetometer that exploits the electromagnetically-induced-transparency (EIT) method for determining a small change in a magnetic field indirectly via measurement of the shift, induced by that change, in the hyperfine levels of resonant atoms exposed to the field.

One of the key components of a magnetometer of this type is a collection of the aforesaid resonant atoms, which have an energy spectrum that is sensitive to any variation in magnetic field. These atoms are placed in a cell, wherein they are irradiated with light from a quantum source (see figure), such that the interactions between the light and the atoms produce a beam of coherent or entangled photons suitable for use in determining the magnetic



An **Optical EIT Magnetometer** according to the proposal would be based on the same measurement principle as that of a state-of-the-art optical EIT magnetometer, but the resonant atoms would be embedded in a photonic crystal such that the variation in the index of refraction with magnetic field would be greatly increased.

field in the cell. If the conditions under which the atoms are exposed are those of EIT, then the shift of Zeeman sub-levels of the atoms caused by a change in the magnetic field results in a change in the index of refraction of the region containing the atoms. The change in the index of refraction is measured by means of a Mach-Zehnder optical interferometer. Then the change in the magnetic field can be computed from the known relationship between the magnetic field and the index of refraction.

A photonic crystal is an engineered periodic dielectric structure that can be

tailored by design to exhibit one or more of a rich variety of optical properties. Notable among these properties is a range of photon energies, known as the photonic band gap (PBG), in which light cannot propagate. In an optical EIT magnetometer according to the proposal, sensitivity would be increased by using a photonic crystal to control and enhance the interaction between the resonant atoms and the optical beam. A cloud of the resonant atoms would be embedded in a photonic crystal rather than in a uniform dielectric material in a cell as in a state-of-the-art

optical EIT magnetometer of prior design. The photonic crystal would be designed so that the photon frequency at the edge of the PBG would closely approximate the atomic transition frequency. In the PBG-edge region, the variation of the index of refraction with a change in the magnetic field would be orders of magnitude greater than in the absence of the photonic crystal.

*This work was done by Igor Kulikov and Lucia Florescu of Caltech for NASA's Jet Propulsion Laboratory. For further information, contact [iaoffice@jpl.nasa.gov](mailto:iaoffice@jpl.nasa.gov). NPO-43802*

## WGM-Resonator/Tapered-Waveguide White-Light Sensor Optics

Light patterns formed by these optics contain information on absorption spectra.

*NASA's Jet Propulsion Laboratory, Pasadena, California*

Theoretical and experimental investigations have demonstrated the feasibility of compact white-light sensor optics consisting of unitary combinations of (1) low-profile whispering-gallery-mode (WGM) resonators and (2) tapered rod optical waveguides. These sensors are highly wavelength-dispersive and are expected to be especially useful in biochemical applications for measuring absorption spectra of liquids.

These sensor optics exploit the properties of a special class of non-diffracting light beams that are denoted Bessel beams because their amplitudes are proportional to Bessel functions of the radii from their central axes. High-order Bessel beams can have large values of angular momentum. In a sensor optic of this type, a low-profile WGM resonator that supports modes having large angular momenta is used to generate high-order Bessel beams. As used here, "low-profile" signifies that the WGM resonator is an integral part of the rod optical waveguide but has a radius slightly different from that of the adjacent part(s).

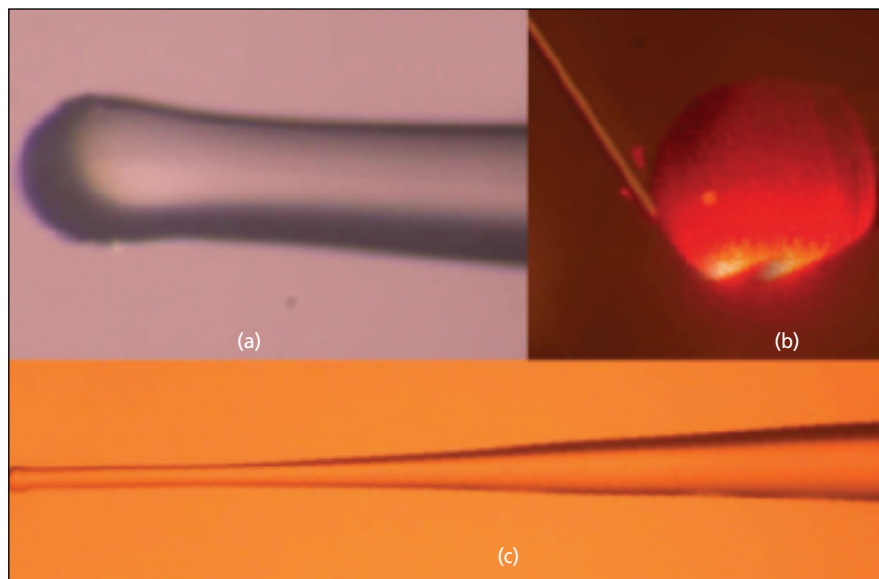
An important difference between such an optic and an ordinary WGM resonator is that its modes decay primarily into Bessel modes of the optical waveguide, rather than to the outside. By changing the dimensions and shape of the WGM resonator and/or the radius of the adjacent part(s) of waveguide, it is possible to change the resonator loading and thereby tailor the degree to which

light propagates from the resonator along the waveguide.

The feasibility of applications that involve exploitation of optical waves that have angular momentum depends on the propagation distances of such waves in free space. A high-order Bessel beam that propagates from a WGM resonator along a cylindrical waveguide with evanescent-field coupling cannot leave the waveguide; it propagates to an end of the waveguide, where it is totally internally reflected back along the waveguide toward the other end. However, if

the waveguide is tapered, as in an optic of the present type, then the optic acts as radiator horn that preserves the angular momentum of the axially propagating Bessel beams while changing their axial momentum. A notable result of propagation along the taper is that upon reaching the wide end, the Bessel beams can be released into the space outside the waveguide and their shapes are preserved.

An optic of the present type can be made by cutting and polishing a bump/dip toroidal pattern on the side



An **Experimental Optic** of the type described in the text is a unitary structure consisting of a WGM resonator on the narrow end of a tapered fused-silica rod: (a) WGM resonator, (b) coupling light into the WGMs of the resonator using cleaved fiber, and (c) tapered fiber used to release generated Bessel beam into free space.

of a rod of transparent material or partly melting the tip of the rod. For example, the figure depicts such an optic made from a fused-silica rod of 30-mm length that tapers from 0.45-mm diameter at the narrow end to 3 mm at the wide end. The WGM resonator is a 500- $\mu\text{m}$  axisymmetric bulge at the narrow end, formed by using a hydrogen torch to partly melt the narrow end. In operation, light is coupled into the WGM

resonator via the cleaved tip of an optical fiber.

In use of such an optic as a sensor, the rod is dipped into liquid, the absorption spectrum of which one seeks to measure. Interference among the Bessel beams in the far-field region of the waveguide forms a helix-shaped light field. A charge-coupled-device camera is installed at a distance between 2 and 30 mm from the wide end of the optical fiber to observe

this field. The dependence of the brightness of this field on the azimuth angle contains information on absorption as a function of wavelength.

*This work was done by Dmitry Strelakov, Lute Maleki, Andrey Matsko, Anatoliy Savchenkov, and Vladimir Itchenko of Caltech for NASA's Jet Propulsion Laboratory. Further information is contained in a TSP (see page 1). NPO-43363*

## Raman-Suppressing Coupling for Optical Parametric Oscillator

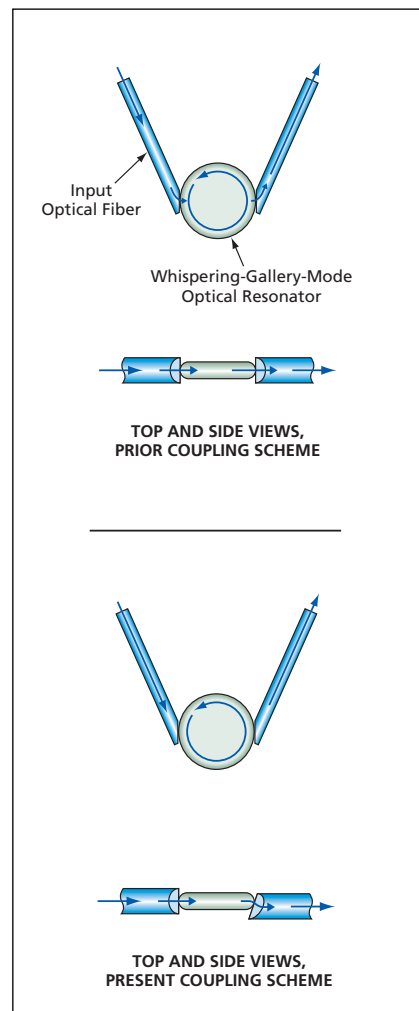
Loading of desired modes is reduced, relative to loading of undesired modes.

NASA's Jet Propulsion Laboratory, Pasadena, California

A Raman-scattering-suppressing input/output coupling scheme has been devised for a whispering-gallery-mode optical resonator that is used as a four-wave-mixing device to effect an all-optical parametric oscillator. Raman scattering is undesired in such a device because (1) it is a nonlinear process that competes with the desired nonlinear four-wave conversion process involved in optical parametric oscillation and (2) as such, it reduces the power of the desired oscillation and contributes to output noise.

An all-optical parametric oscillator potentially offers the advantages of a narrow output spectral peak with a low overall noise floor. Often, undesirably, the threshold power for Raman scattering is lower than that for optical parametric oscillation, partly because phase matching is not a necessary precondition for Raman scattering. On the other hand, phase matching is necessary for four-wave mixing, in which pump power in fundamental modes of the resonator is converted to only fundamental modes of a different frequency. Some of the pump laser power needed for optical parametric oscillation can be Raman-scattered to non-fundamental modes of the resonator. The resonance quality factors ( $Q$  values) of these non-fundamental modes are not reduced by the presence of input and output fiber-optic couplers designed according to a prior coupling scheme, and the threshold power levels of both competing nonlinear processes decrease with increasing  $Q$  values. Moreover, when the pump power reaches the Raman-scattering threshold, the  $Q$  values of the pump modes decrease, with consequent increase in the oscillator output noise. For these reasons, it is

highly desirable to utilize a modified coupling scheme to suppress the Raman modes without significantly suppressing the fundamental modes.



These Two Input/Output Coupling Schemes differ in the position and orientation of the output optical fiber. In the present scheme, the output fiber is tilted to reduce coupling to the fundamental modes of the resonator.

The essence of the present input/output coupling scheme is to reduce output loading of the desired resonator modes while increasing output loading of the undesired ones. The figure illustrates the prior and present coupling schemes. In the prior scheme, the input and output couplers are both positioned and oriented to effect coupling to the fundamental modes of the resonator. The  $Q$  of the fundamental modes is reduced by this coupling — especially by output coupling to the load. In the present scheme, the input coupler is still positioned and oriented to effect coupling to the fundamental modes, but the output coupler is tilted to greatly reduce coupling to the fundamental modes without reducing coupling to the Raman modes. As a result, the  $Q$  values of the fundamental modes are increased while the output loading reduces the  $Q$  values (and thereby increases the threshold power) of the Raman modes.

*This work was done by Anatoliy Savchenkov, Lute Maleki, Andrey Matsko, and Enrico Rubiola of Caltech for NASA's Jet Propulsion Laboratory. Further information is contained in a TSP (see page 1).*

*In accordance with Public Law 96-517, the contractor has elected to retain title to this invention. Inquiries concerning rights for its commercial use should be addressed to:*

*Innovative Technology Assets Management  
JPL  
Mail Stop 202-233  
4800 Oak Grove Drive  
Pasadena, CA 91109-8099  
(818) 354-2240*

*E-mail: iaoffice@jpl.nasa.gov  
Refer to NPO-44471, volume and number of this NASA Tech Briefs issue, and the page number.*

## CO<sub>2</sub>-Reduction Primary Cell for Use on Venus

NASA's Jet Propulsion Laboratory, Pasadena, California

A document proposes a CO<sub>2</sub>-reduction primary electrochemical cell as a building block of batteries to supply electric power on the surface of Venus. The basic principle of the proposed cell is similar to that of terrestrial Zn-air batteries, the major differences being that (1) the anode metal would not be Zn and (2) CO<sub>2</sub>, which is about 96.5 mole percent of the Venusian atmosphere, would be used, instead of O<sub>2</sub>, as the source of oxygen. The cell would in-

clude a solid electrolyte that could withstand operation at a temperatures as high as 1,000 °C and, hence, could withstand operation at the Venusian surface temperature of ≈460 °C.

Electrical energy would be generated by a combination of (1) electrochemical reduction of CO<sub>2</sub> at the cathode and (2) oxidation of a suitable metal to metal oxide at the anode. Unlike some other types of cells that have been considered for use on Venus, the CO<sub>2</sub>-re-

duction cell could operate for a long time, without need for cooling. If the anode metal were Mg, then the performance could be impressive: The specific energy of the proposed cell has been estimated theoretically to be 3.46 W·h/g.

*This work was done by William West, Jay Whitacre, and Sekharipuram Narayanan of Caltech for NASA's Jet Propulsion Laboratory. Further information is contained in a TSP (see page 1). NPO-40892*

## Cold Atom Source Containing Multiple Magneto-Optical Traps

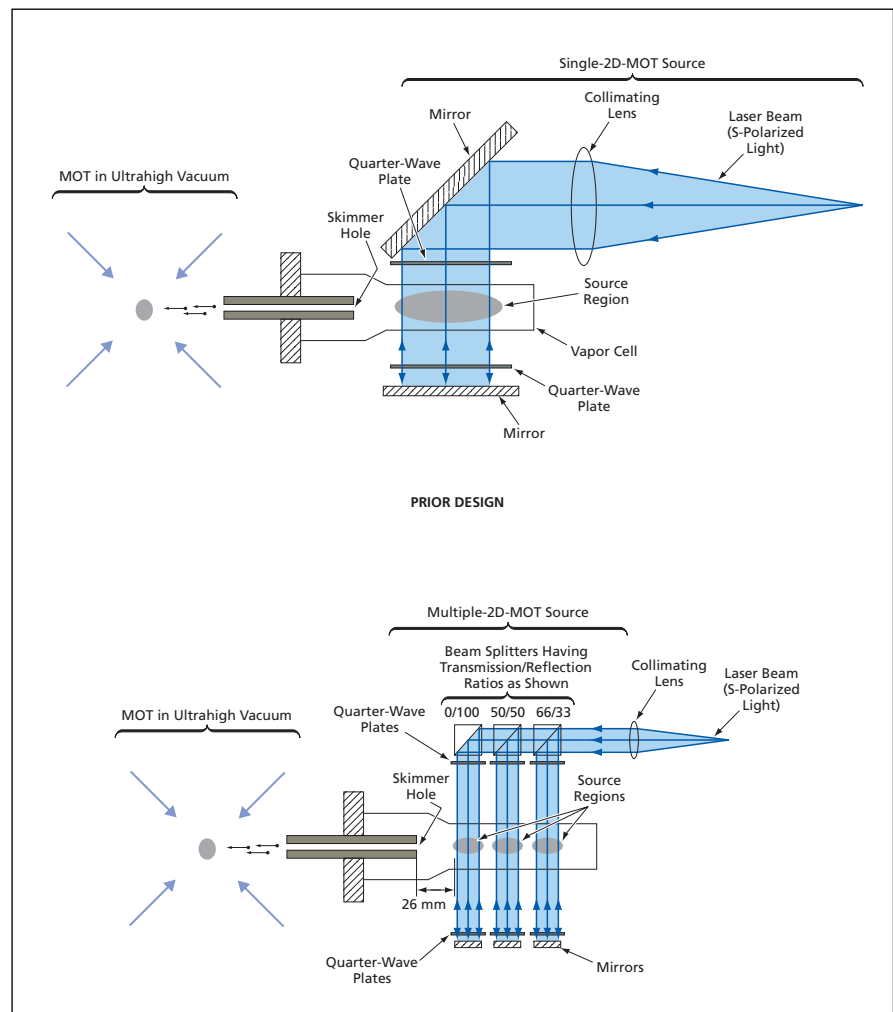
This source allows a smaller package relative to single-trap sources of similar performance.

NASA's Jet Propulsion Laboratory, Pasadena, California

An apparatus that serves as a source of a cold beam of atoms contains multiple two-dimensional (2D) magneto-optical traps (MOTs). (Cold beams of atoms are used in atomic clocks and in diverse scientific experiments and applications.) The multiple-2D-MOT design of this cold atom source stands in contrast to single-2D-MOT designs of prior cold atom sources of the same type. The advantages afforded by the present design are that this apparatus is smaller than prior designs.

The figure schematically depicts a prior single-2D-MOT source and the present multiple-2D-MOT source. (It should be noted that the 2D nature of these sources lies in an aspect of the optics that has been omitted from the figure for the sake of simplicity. The plane of the figure corresponds to one of two planes of incidence. The other plane of incidence, perpendicular to the plane of the figure and coincident with the horizontal axis of the source region, contains a set of optics identical to those shown here.)

In the single-2D-MOT apparatus, a cell that is otherwise evacuated contains a vapor of atoms at a regulated low pressure. Slower atoms are collected in the source region by the magneto-optical trapping action. A cold beam of atoms leaves the trapping region by passing through a skimmer hole, along a graphite-getter-lined differential pumping tube, into an MOT in an ultrahigh vacuum wherein the atoms are utilized.



These Simplified Schematic Diagrams of two cold atom sources highlight some of the main differences between the single- and multiple-2D-MOT designs.

The present multiple-2D-MOT apparatus works similarly, except that multiple smaller 2D MOTs that form shorter source regions are concatenated to form the equivalent of a single longer 2D MOT source region. In each of the two planes of incidence, the multiple laser beams needed for the multiple traps are generated from a single input laser beam by use of a stack of beam splitters.

The advantages of compactness of the present design arise as follows: In the prior single-2D-MOT case, the overall linear dimensions of the optics and the laser beam equal or exceed the length of the source region. In the present multiple-2D-MOT case, the laser beams can be narrower and, hence, the optics can be smaller. One can, if necessary, create a longer source region for higher cold atom flux, with-

out using wider laser beams and without widening the overall apparatus, by adding 2D MOTs and correspondingly modifying the optics to include more beam splitters.

*This work was done by Jaime Ramirez-Serrano, James Kohel, James Kellogg, Lawrence Lin, Nan Yu, and Lute Maleki of Caltech for NASA's Jet Propulsion Laboratory. For further information, contact [iaoffice@jpl.nasa.gov](mailto:iaoffice@jpl.nasa.gov). NPO-41242*





## POD Model Reconstruction for Gray-Box Fault Detection

Low-order models that give robust, close approximations can be constructed.

NASA's Jet Propulsion Laboratory, Pasadena, California

Proper orthogonal decomposition (POD) is the mathematical basis of a method of constructing low-order mathematical models for the "gray-box" fault-detection algorithm that is a component of a diagnostic system known as beacon-based exception analysis for multimissions (BEAM). POD has been successfully applied in reducing computational complexity by generating simple models that can be used for control and simulation for complex systems such as fluid flows. In the present application to BEAM, POD brings the same benefits to automated diagnosis.

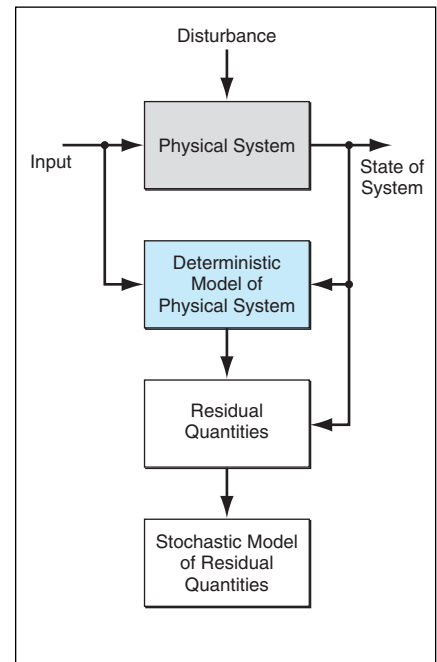
Selected aspects of BEAM have been described in numerous prior NASA Tech Briefs articles. To summarize briefly: BEAM is a method of real-time or off-line, automated diagnosis of a complex dynamic system. The gray-box approach makes it possible to utilize incomplete or approximate knowledge of the dynamics of the system that one seeks to diagnose. In the gray-box approach, a deterministic model of the system is used to filter a time series of system sensor data to remove the deterministic components of the time series from further examination. What is left after the filtering operation is a time series of residual quantities that represent the unknown (or at least unmodeled) aspects of the behavior of the system. Stochastic modeling techniques are then applied to the residual time series (see figure). The procedure for detecting abnormal behavior of the system then becomes one of looking for statistical differences between the resid-

ual time series and the predictions of the stochastic model.

The need for POD or another method to construct simple approximate models for use in the gray-box approach arises because in a typical case, a detailed deterministic model of the system to be diagnosed may not exist, or, if it exists, may be too complex for real-time computations. One or more simplified deterministic model(s) that describe the system to acceptable degrees of accuracy are therefore desired. The simplified deterministic models can be created from computational simulations of the system and/or empirical data on the operation of the system.

POD modeling requires two steps. The first step is to extract the "mode shapes" or basis functions from experimental data or detailed simulations of the system. This step can involve principal-component analysis, i.e., singular-value decomposition. In the second step, the basis functions are projected to a low-order or few-dimensional approximate dynamical model by use of the Galerkin method.

The present POD-based method has been verified by creating a low-order dynamical model of a system represented by Burgers' equation, which is a partial differential equation that describes a diverse set of wave phenomena such as flowing gases, flood waters, glaciers, and automobile traffic. It was demonstrated that a low-order (7 POD modes) dynamical model that exhibited high fidelity could be created, even in the presence of



In the **Gray-Box Method**, the present POD-based method is used to construct a low-order deterministic model that closely approximates the behavior of the physical system.

noise. In the absence of noise, the model was found to simulate the system with 1 percent error. In the presence of 10-percent uncorrelated Gaussian noise, the model was found to simulate the system with 5 percent error.

*This work was done by Han Park and Michail Zak of Caltech for NASA's Jet Propulsion Laboratory. For more information, contact iaoffice@jpl.nasa.gov. NPO-30871.*

## System for Estimating Horizontal Velocity During Descent

Estimates are generated from images and other sensor outputs.

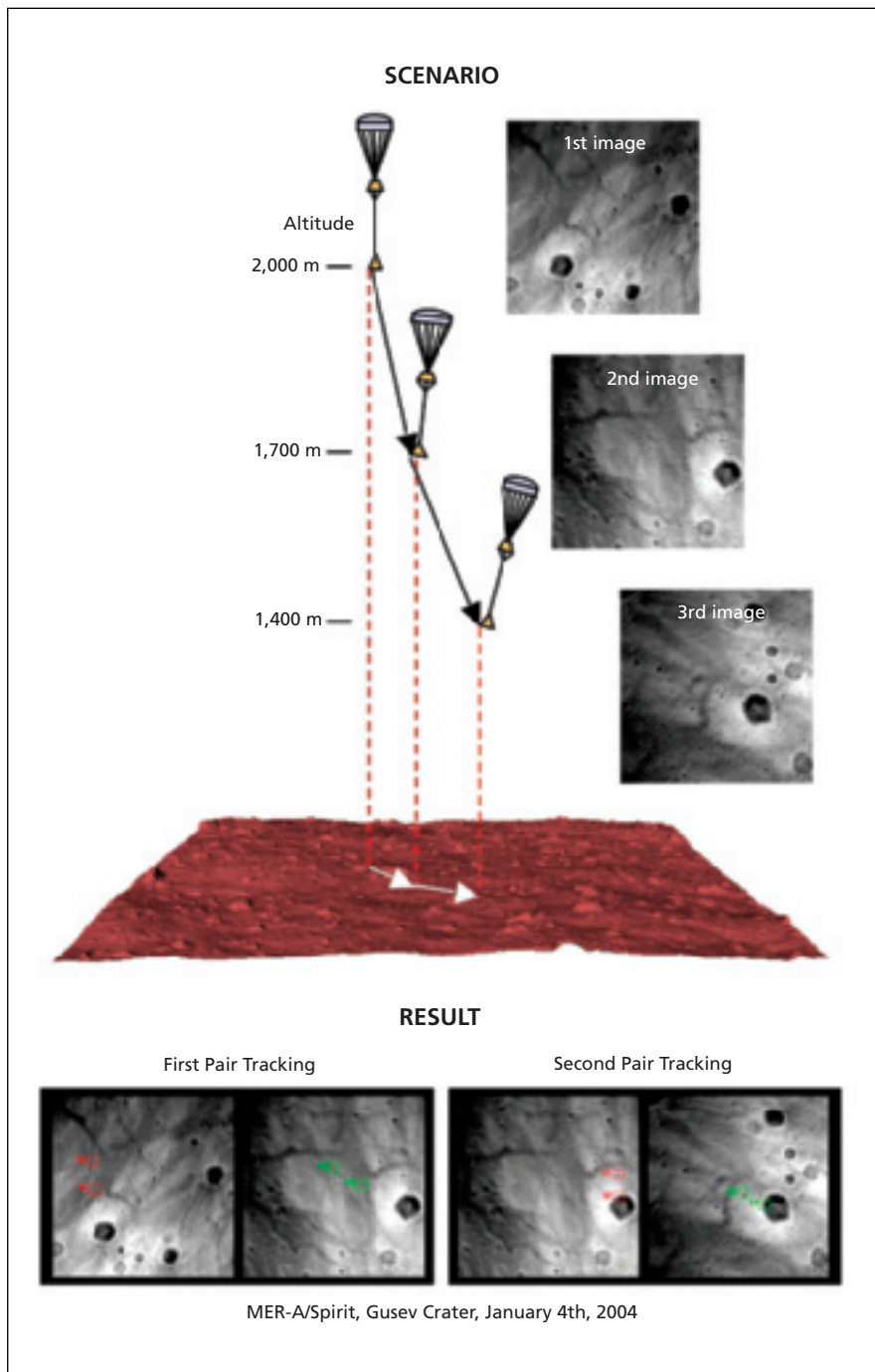
NASA's Jet Propulsion Laboratory, Pasadena, California

The descent image motion estimation system (DIMES) is a system of hardware and software, designed for original use in estimating the horizontal velocity of a spacecraft descending toward a landing

on Mars. The estimated horizontal velocity is used in generating rocket-firing commands to reduce the horizontal velocity as part of an overall control scheme to minimize the landing impact.

DIMES can also be used for estimating the horizontal velocity of a remotely controlled or autonomous aircraft for purposes of navigation and control.

DIMES was developed by the Mars Ex-



The **DICES Algorithm** fuses images of terrain below with IMU data and radar-altimeter readings to estimate horizontal velocity.

ploration Rover (MER) Project and was used successfully by the MER Entry Descent and Landing (EDL) system during both landings. In the original spacecraft application, when the need to determine horizontal velocity was discovered,

it was too late to install traditional horizontal-velocity-measuring radar in the spacecraft. DICES was conceived as a means of estimating the horizontal velocity by augmenting data acquired by sensors already installed in the space-

craft with data from an easy to accommodate descent imager.

The DICES sensors include a descent imager (an electronic camera that acquires images of the approaching terrain), a radar altimeter, and an inertial measurement unit (IMU). The DICES flight software implements an algorithm for combining measurement data from the aforementioned sensors to estimate horizontal velocity.

The input required by the DICES software includes three descent images. For each descent image, the software also requires the following elements of the state of the landing spacecraft at times when the images were acquired: the attitude of the spacecraft relative to the surface, the horizontal velocity estimated by the IMU, and the altitude. Using this state information, the software warps each image to the ground plane, then computes horizontal displacements between successive images by use of image correlation, applied to two locations in each of the first and second images and two locations in each of the second and third images. This process yields four image-based estimates of horizontal velocity. These estimates are compared to each other for consistency. As a further consistency check, accelerations are computed from differences of these velocities and these accelerations are compared with accelerations as measured by the IMU.

The results of the consistency checks are used, along with image-correlation metrics to decide whether the estimate of horizontal velocity is correct. In the original application, if the estimate of velocity is determined to be correct, it is sent to the rocket-firing subsystem; if the estimate of horizontal velocity is found to be incorrect, then the rocket-firing subsystem is commanded to proceed without a DICES velocity estimate.

*This work was done by Andrew Johnson, Yang Cheng, Reg Willson, Jay Goguen, Alejandro San Martin, Chris Leger, and Larry Matthies of Caltech for NASA's Jet Propulsion Laboratory.*

*The software used in this innovation is available for commercial licensing. Please contact Karina Edmonds of the California Institute of Technology at (626) 395-2322. Refer to NPO-40920.*



## Software Framework for Peer Data-Management Services

Object Oriented Data Technology (OODT) is a software framework for creating a Web-based system for exchange of scientific data that are stored in diverse formats on computers at different sites under the management of scientific peers. OODT software consists of a set of cooperating, distributed peer components that provide distributed peer-to-peer (P2P) services that enable one peer to search and retrieve data managed by another peer. In effect, computers running OODT software at different locations become parts of an integrated data-management system.

OODT now incorporates a client/server communication substrate, but in other respects, its design resembles that of a P2P network, and it is planned to make a transition to a P2P communication substrate in the near future. OODT uses standard Transmission Control Protocol/ Internet Protocol (TCP/IP) connections. The architecture of OODT is that of a plug-in system. The OODT framework includes a set of classes and interfaces that can be customized and then registered with an application programmer's interface. The classes and interfaces tell the programmer at each site exactly what is needed for customization.

*This program was written by John Hughes, Sean Hardman, Daniel Crichton, and Jason Hyon of Caltech and Sean Kelly and Thuy Tran of Northrop Grumman for NASA's Jet Propulsion Laboratory.*

*This software is available for commercial licensing. Please contact Karina Edmonds of the California Institute of Technology at (626) 395-2322. Refer to NPO-40370.*

## Autogen Version 2.0

Version 2.0 of the autogen software has been released. "Autogen" (automated sequence generation) signifies both a process and software used to implement the process of automated generation of sequences of commands in a standard format for uplink to spacecraft. Autogen requires fewer workers than are needed for older manual sequence-generation processes and reduces sequence-generation times from weeks to minutes.

The autogen software comprises the autogen script plus the Activity Plan Generator (APGEN) program. APGEN can be used for planning missions and command sequences. APGEN generates a graphical user interface that facilitates scheduling of activities on a time line and affords a capability to automatically expand, decompose, and schedule activities. The earlier version of the autogen software was developed for the Mars 2001 *Odyssey* spacecraft. Version 2.0 offers enhanced capabilities to serve, simultaneously, multiple spacecraft (including the Mars Global Surveyor, the Mars Exploration Rovers, and the future Mars Reconnaissance Orbiter) that may be at different phases of their missions (including cruise, aerobraking, mapping, and relay operations).

*This work was done by Roy Gladden of Caltech for NASA's Jet Propulsion Laboratory. Further information is contained in a TSP (see page 1).*

*This software is available for commercial licensing. Please contact Karina Edmonds of the California Institute of Technology at (626) 395-2322. Refer to NPO-41501.*

## Tracking-Data-Conversion Tool

A computer program denoted Tracking Data Delivery Software Orbit Data File (TDDSODF) converts deep-space-radio-communication spacecraft-tracking data from a currently used file format known in the art as "TRK-2-34" to a legacy format denoted "TRK-2-18." TDDSODF reads standard formatted data units (SFDUs) of several TRK-2-34 types and processes them into an orbit data file (ODF) containing data of one or more of several different TRK-2-18 types. TDDSODF offers the user the following options:

- To set processing parameters (including default values for use when TRK-2-34 values are not available) through configuration files or from a command line,
- To specify a compression interval used in the generation of carrier-frequency observables from TRK-2-34 downlink-carrier-phase and Doppler-count SFDUs,
- To fix the formulation of observables to a time-tag that is an integer multiple of a user-specified interval,
- To verify whether the configuration

files contain valid keywords or out-of-range keyword values, and

- To specify both required and optional command-line parameters in a single file.

*This program was written by Dana Flora-Adams, Jeanne Makihara, Zabel Benenyam, Jeff Berner, and Andrew Kwok of Caltech for NASA's Jet Propulsion Laboratory.*

*This software is available for commercial licensing. Please contact Karina Edmonds of the California Institute of Technology at (626) 395-2322. Refer to NPO-41741.*

## NASA Enterprise Visual Analysis

NASA Enterprise Visual Analysis (NEVA) is a computer program undergoing development as a successor to Launch Services Analysis Tool (LSAT), formerly known as Payload Carrier Analysis Tool (PCAT). NEVA facilitates analyses of proposed configurations of payloads and packing fixtures (e.g. pallets) in a space-shuttle payload bay for transport to the International Space Station. NEVA reduces the need to use physical models, mock-ups, and full-scale ground support equipment in performing such analyses. Using NEVA, one can take account of such diverse considerations as those of weight distribution, geometry, collision avoidance, power requirements, thermal loads, and mechanical loads.

NEVA accepts mass-property data from computational models of payloads, carriers, and interfaces, and uses these data to perform weight and center-of-gravity analyses. NEVA accepts results from structural, thermal, and fluid-analysis programs and translates them for incorporation into visual displays along with the results of the weight-distribution analyses. After contemplated further development, NEVA will also be able to accept, translate, and display results of communication- and electromagnetic-compatibility-analysis programs. Thus, NEVA is expected to continue to evolve into an increasingly capable tool for supporting technical and management decisions regarding ever more complex payload configurations.

*This program (copyright © The Boeing Company 2005, all rights reserved) was written by Maria Lopez-Tellado of Kennedy Space Center and Brenda DiSanto, Robert Humeniuk, Richard Bard Jr., Mia Little, Robert Edwards, Tien-Chi Ma, Kenneth*

Hollifield, and Chuck White of The Boeing Co. GSA-23F-0183K, Order No. NNK04MB84D.

Inquiries concerning licenses for its commercial development should be addressed to:

Terrance Mason, Boeing Patent Licensing Professional

Boeing Management Company

Mail Stop 1650-7002 Laguna Canyon Road  
Irvine, CA 92618

Phone No.: (949) 790-1331

E-mail: [terrance.mason@boeing.com](mailto:terrance.mason@boeing.com)

Refer to Boeing Docket No 03-1523

Web site: <http://www.boeing.com>

KSC-12712

---

## Advanced Reference Counting Pointers for Better Performance

A computer program implements reference counting pointers (RCPs) that are lock-free, thread-safe, async-safe, and operational on a multiprocessor computer. RCPs are powerful and convenient means of managing heap memory in C++ software. Most prior RCP programs use locks to ensure thread safety and manage concurrency. The present program was developed in a continuing effort to explore ways of using the C++ programming language to develop safety-critical and mission-critical software.

This effort includes exploration of lock-free algorithms because they offer potential to avoid some costly and difficult verification problems. Unlike previously published RCP software, the present program does not use locks (meaning that no thread can block progress on another thread): Instead, this program implements algorithms that exploit capabilities of central-processing-unit hardware so as to avoid locks. Once locks are eliminated, it becomes possible to realize the other attributes mentioned in the first sentence. In addition to the abovementioned attributes, this program offers several advantages over other RCP programs that use locks: It is smaller (and, hence, is faster and uses less memory), it is im-

mune to priority inversion, and there is no way for it to cause a C++ exception.

This program was written by William Reinholdt of Caltech for NASA's Jet Propulsion Laboratory.

In accordance with Public Law 96-517, the contractor has elected to retain title to this invention. Inquiries concerning rights for its commercial use should be addressed to:

Innovative Technology Assets Management  
JPL

Mail Stop 202-233

4800 Oak Grove Drive

Pasadena, CA 91109-8099

(818) 354-2240

E-mail: [iaoffice@jpl.nasa.gov](mailto:iaoffice@jpl.nasa.gov)

Refer to NPO-41196, volume and number of this NASA Tech Briefs issue, and the page number.

---

## C Namelist Facility

C Namelist Facility (CNL) is a package of software that supports the development of data-driven programs that utilize relatively free-form input files (e.g., text files) to control complex operations. The only comparable prior namelist facility is built into Fortran and does not support arrays or records. Newer computing languages, including C and Pascal, do not include built-in namelist facilities. A namelist facility enables a program to utilize relatively free-form input files that contain assignment statements that give values to variables. Variables to which values are not assigned in input files remain unchanged; therefore, it becomes possible to have default values set by static or dynamic initialization of values prior to namelist input and updating of values is optional. Because it is not required to include values of variables in namelist input files, new parameters can be added to evolving programs without rendering old namelist input files obsolete — provided that the new parameters have useful default values. It should be possible to execute CNL in any operating system that supports the ANSI C programming language. It has been ex-

ecuted in several variants of Unix and in VxWorks.

This program was written by Bruce Bon of Caltech for NASA's Jet Propulsion Laboratory.

This software is available for commercial licensing. Please contact Karina Edmonds of the California Institute of Technology at (626) 395-2322. Refer to NPO-40087.

---

## Efficient Mosaicking of Spitzer Space Telescope Images

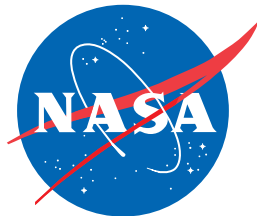
A parallel version of the MOPEX software, which generates mosaics of infrared astronomical images acquired by the Spitzer Space Telescope, extends the capabilities of the prior serial version. In the parallel version, both the input image space and the output mosaic space are divided among the available parallel processors. This is the only software that performs the point-source detection and the rejection of spurious imaging effects of cosmic rays required by Spitzer scientists. This software includes components that implement outlier-detection algorithms that can be fine-tuned for a particular set of image data by use of a number of adjustable parameters.

This software has been used to construct a mosaic of the Spitzer Infrared Array Camera Shallow Survey, which comprises more than 17,000 exposures in four wavelength bands from 3.6 to 8  $\mu\text{m}$  and spans a solid angle of about 9 square degrees. When this software was executed on 32 nodes of the 1,024-processor Cosmos cluster computer at NASA's Jet Propulsion Laboratory, a speedup of 8.3 was achieved over the serial version of MOPEX. The performance is expected to improve dramatically once a true parallel file system is installed on Cosmos.

This program was written by Joseph Jacob, David Makovoz, and Peter Eisenhardt of Caltech for NASA's Jet Propulsion Laboratory.

This software is available for commercial licensing. Please contact Karina Edmonds of the California Institute of Technology at (626) 395-2322. Refer to NPO-42860.





National Aeronautics and  
Space Administration